LBL-23195 c.2
UC-11

Lawrence Berkeley Laboratory
UNIVERSITY OF CALIFORNIA

EARTH SCIENCES DIVISION

RECEIVED
LAWRENCE
BERKELEY LABORATORY

JUL 31 1987

LIBRARY AND
DOCUMENTS SECTION

CHANNELING CHARACTERISTICS OF FLOW AND SOLUTE TRANSPORT THROUGH A ROUGH-SURFACED FRACTURE

Y.W. Tsang, C.F. Tsang, F.V. Hale,
L. Moreno, and I. Neretnieks

June 1987

TWO-WEEK LOAN COPY

This is a Library Circulating Copy which may be borrowed for two weeks.

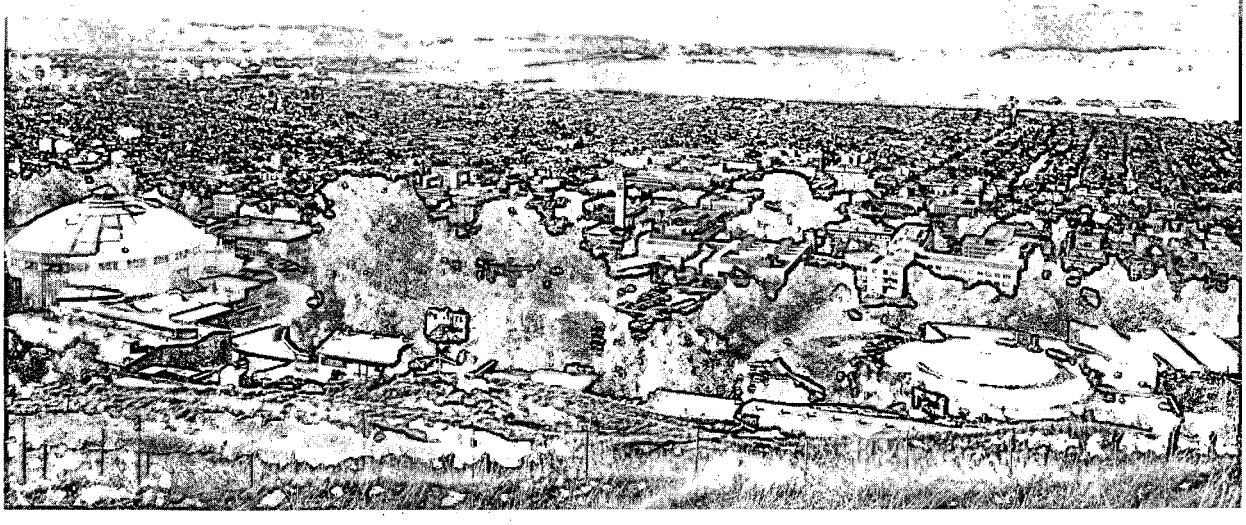

Prepared for the U.S. Department of Energy under Contract DE-AC03-76SF00098

LBL-23195 c.2

DISCLAIMER

This document was prepared as an account of work sponsored by the United States Government. While this document is believed to contain correct information, neither the United States Government nor any agency thereof, nor the Regents of the University of California, nor any of their employees, makes any warranty, express or implied, or assumes any legal responsibility for the accuracy, completeness, or usefulness of any information, apparatus, product, or process disclosed, or represents that its use would not infringe privately owned rights. Reference herein to any specific commercial product, process, or service by its trade name, trademark, manufacturer, or otherwise, does not necessarily constitute or imply its endorsement, recommendation, or favoring by the United States Government or any agency thereof, or the Regents of the University of California. The views and opinions of authors expressed herein do not necessarily state or reflect those of the United States Government or any agency thereof or the Regents of the University of California.

LBL-23195

CHANNELING CHARACTERISTICS OF FLOW AND SOLUTE TRANSPORT THROUGH A ROUGH-SURFACED FRACTURE

Y. W. Tsang, C. F. Tsang , F. V. Hale

Earth Sciences Division
Lawrence Berkeley Laboratory
University of California
Berkeley, California 94720

L. Moreno and I. Neretnieks

Department of Chemical Engineering
Royal Institute Of Technology
Stockholm, Sweden

June 1987

Channeling Characteristics of Flow and Solute Transport through a Rough-Surfaced Fracture

Y. W. Tsang, C. F. Tsang, F. V. Hale

Earth Sciences Division
Lawrence Berkeley Laboratory
University of California
Berkeley, California 94720

L. Moreno and I. Neretnieks

Department of Chemical Engineering
Royal Institute Of Technology
Stockholm, Sweden

ABSTRACT

Calculations for the flow and solute transport through a single rough-surfaced fracture are carried out. The fracture plane is discretized into square meshes to which variable apertures are assigned. The spatially varying apertures in the single fractures are generated using geostatistical methods, based on a given aperture density distribution and a specified spatial correlation length. Constant head boundary conditions are assumed for the flow in the single fracture. The fluid potential at each mesh intersection is computed and the steady state flowrates between all adjacent meshes are obtained. The calculations for flow in two-dimensions show that fluid flows unevenly in a single fracture, and that it takes place in a few preferred paths. The solute transport is calculated using a particle tracking method. The channeling characteristics of fluid flow and solute transport phenomena as a function of the fracture geometry (aperture density distribution and spatial correlation length) is demonstrated; and the implication to experimental measurements are discussed. The two-dimensional solute transport results are then interpretated in terms of a one-dimensional channel model: a system of independent variable-aperture channels acting as flow paths for the solute transport. The result that the two-dimensional breakthrough curves are reproducible by the one-dimensional conceptual model sheds much light on the potential utility of the simple one-dimensional channel model to interpret flow and solute transport in both two- and three-dimensional fractured systems. This approach entails an enormous saving of computation effort.

INTRODUCTION

In flow through low permeability fractured media, for both the laboratory and field scales, there are evidences that flow takes place in a limited number of preferred paths. This kind of channeling phenomena have been observed in both the flow through a single fracture (Pyrak et al., 1985; Abelin et al., 1983; 1985; Bourke, 1987) and in a multifractured medium (Neretnieks, 1985). Where channeling of flow through fractures is observed, it is clear that a porous medium description will be quite inadequate in representing the fluid flow behavior in the medium. Under these circumstances, we have described a theoretical approach (Tsang and Tsang, 1987) to treat the fluid flow as through channels. These channels have variable apertures along its length, the apertures of all the channels obey a given aperture density distribution function, and the spatial variation of the apertures along each channel is governed by the same spatial correlation length, λ. We have made the further assumption that the width of the channels is typically one spatial correlation length, and that the apertures within the channel width take on a constant average value. Such an assumption reduces the flow problem to one of flow through a system of one-dimensional, tortuous channels with variable apertures along their lengths.

The basic hypothesis of the channel model is that for a given experiment the data may be analyzed as if flow and transport had taken place in a system of channels that are statistically equivalent, that is, the channels are described by the same aperture density distribution and the spatial correlation length. The channels generated from a given aperture density distribution and spatial correlation have the property that their volumes per unit length are similar, yet the flow rates and residence times of tracer can vary over a range of several orders of magnitude, due to the finite probability of the occurrence of very small apertures along some of the channels (Tsang et al., 1987). This channel model which describes flow and transport in two and three dimension by a system of independent one-dimensional channels simplifies the computational effort enormously. Current approaches for calculation of steady flow in a heterogeneous medium involve discretization of the medium into an appropriate mesh of nodes and elements, then solving the Laplace equation for fluid potentials. For large scale problems in two

and three dimensions, this often demands the handling of very large matrices and may exceed the storage capacity of even large computers. When storage is not a problem, the computation may still be prohibitively time consuming. The conceptual channel model of interpreting flow and transport data in terms of one-dimensional flow paths was intended to sidestep these computation difficulties by incorporating as much physics as possible into the model. The notion of solving directly for the flow paths of a heterogenous medium, as opposed to the conventional way of solving for the fluid potentials, has also been suggested by Narasimhan (1985).

In the present work, we present our investigations of flow in two dimensions, corresponding to the physical situation of flow in single fractures. The purpose of this paper is three-fold. First, by solving for the flow exactly by Laplace equation in two-dimensions, we would like to understand the flow characteristics in single fractures and to identify the key parameters that control the channeling flow pattern, thus affording a way to interpret single fracture field and laboratory experiments by Pyrak et al. (1985), Abelin et al. (1983, 1985) and Bourke (1987), all of which exhibit channeling behavior. Second, the results of the present calculations in two-dimension shed light on the validity of some of the simplifying assumptions in the conceptual channel model (Tsang and Tsang, 1987), where we proposed one dimensional channel representation of flow in both two- and three-dimensions when interpretating data. Third, since the preferred flow paths or channels in three dimensional fractured media are probably composed of connected paths in system of intersecting single fractures, the implications of our present two-dimensional calculations on field tests in three-dimension will be discussed.

FLOW AND TRANSPORT IN TWO DIMENSIONS

Fracture Aperture Generation

Here we outline the numerical model to calculate the fluid flow and solute transport through a single fracture with variable apertures. The fracture plane is partitioned by grids with a different aperture assigned to each square enclosed by grid lines. The

assignment of the apertures is by means of geostatistical method which generates two-dimensional field of a correlated distributed parameter. Little data is available on the actual distribution of apertures in a single fracture. Surface profiling measurements on 12 cm cores of a natural fracture in granite (Gentier, 1986) seem to indicate that the apertures follow a gamma distribution (Tsang and Tsang, 1987). Apparent apertures that have been observed in cores or well logs measured by Bianchi and Snow (1968); and apertures derived from permeability tests in granite (Bourke et al., 1985) were found to follow a lognormal distribution. For the purpose of this study, the exact form of aperture density distribution and covariance function are not critical, we chose a lognormal distribution for the variable apertures in the plane of the single fracture and exponential function for the spatial covariance of the apertures. We used the numerical code COVAR (Williams and El-Kadi, 1986) to generate different aperture values in the fracture plane divided into square meshes. COVAR uses the matrix decomposition method to generate the log-normally distributed values of fracture apertures, b, which are first transformed to the normal distribution, Y,

$$Y = \log_{10} b \tag{1}$$

The values of Y are estimated from,

$$Y = L.\epsilon + \nu \tag{2}$$

in which ν is the mean of Y, ϵ is a vector N [0,1] (i.e., normally distributed with mean of zero and standard deviation of 1), and L is defined in terms of the covariant matrix

$$A = LL^T \tag{3}$$

Equation (2) represents the generated process because the mean is given by

$$E\,[Y] = LE\,[\epsilon] + \nu = \nu \tag{4}$$

and the covariance is given by

$$E\,[(Y-\nu)(Y-\nu)^T] = LE\,[\epsilon\epsilon^T]L^T = LL^T = A \tag{5}$$

in which E stands for the expected value. We used the exponential form of the covariance function

$$A=\sigma^2 \exp^{-\alpha |r|} \tag{6}$$

in which σ^2 is the variance of Y, r is the separation lag, and α is the autocorrelation parameter which has the dimension of inverse length. The exponential form of (6) indicates that quantities within distance on the order of $2/\alpha$ will be correlated and thus we may define the correlation length, λ to be $2/\alpha$. The form of (6) indicates that the covariance chosen is isotropic. An anisotropic form of the covariance function may also be chosen.

Figures 1 and 2 show eight realizations of statistically generated apertures with identical mean and variance of the log-normal aperture density distribution: the mean ν=1.7 , and the square root of variance σ=0.43. The mean corresponds to an aperture of $10^{1.7}$ = 50 μm. The square region of unit length in linear dimension therefore represents a single fracture with spatially correlated variable apertures as a flow region. Figure 1 differs from Figure 2 only in the spatial correlation length of the apertures. The correlation length is expressed in terms of a fraction of the linear extent of the square generated region. The spatial variation of the apertures in Figure 1 correspond to a correlation length, λ, of 0.1 of the linear dimension of the fracture flow region, those in Figure 2 all correspond to a λ, of 0.4 of the linear dimension of the fracture flow region. The variation of the apertures is represented by the different shading in Figures 1 and 2, the darker the shading, the smaller the aperture. That the spatial correlation of the apertures are different in Figures 1 and 2 is quite apparent.

Fluid Flow Calculations

The fluid flow through these variable-aperture fractures shall be calculated for the constant pressure head boundary conditions: with reference to the geometry as shown in Figure 3a, the left boundary is kept at a higher potential P_1, the right boundary at a lower potential P_2, with the no flow conditions imposed on the upper and lower boundaries. The steady laminar velocity of a viscous incompressible fluid through a pair of smooth parallel walls separated by a distance b satisfies the equation (e.g., Snow, 1965),

$$\vec{v}=-\frac{1}{12\mu} b^2 \nabla P \tag{7}$$

where $\vec{v}$ is the Darcy velocity, μ the dynamic fluid viscosity, and P is the fluid pressure. Then the volumetric fluid flow is,

$$Q=\frac{1}{12\mu}b^3W\Delta P/L \tag{8}$$

where the pressure drop is Δ P over a length of L and W is the extent of the parallel plates normal to the pressure variation. Equation (8) may be applied to each of the squares enclosed by the grid lines such as shown in Figure 3a. In this regard, we assume that the ratio of aperture to the grid spacing is much smaller than 1, so that convergence or divergence in flow lines near the boundary between two grid squares does not change the simple relationship given in Equation (8). Figure 3b shows a schematic diagram of two adjacent nodes with apertures b_i and b_j respectively. When the volumetric fluid flow rate from node i to node j is Q_{ij}, we can write down the expression for the pressure drop from node i to node j,

$$\begin{aligned} P_i-P_j &= \frac{Q_{ij}}{\frac{1}{12\mu}b_i^3\Delta y\frac{2}{\Delta x}}+\frac{Q_{ij}}{\frac{1}{12\mu}b_j^3\Delta y\frac{2}{\Delta x}} \\ &= Q_{ij}\left[6\mu\frac{\Delta x}{\Delta y}\left(\frac{1}{b_i^3}+\frac{1}{b_j^3}\right)\right] \\ &= Q_{ij}\,R_{ij} \end{aligned} \tag{9}$$

where R_{ij} is the resistance to flow between nodes i and j. The mass balance at each node, i, may be written as

$$\sum_j Q_{ij}=\sum_j\frac{P_i-P_j}{R_{ij}}=0. \tag{10}$$

Except for the nodes at the left and right boundaries of the fracture region, the pressure at each node is an unknown to be solved. The system of Equations (10) with the pressures as unknowns is solved using a sparse matrix solver (NAG Library of Mathematical Routines). The solutions of the system of equations yield the pressure at each node, and flow between adjacent nodes is then calculated using Equation (9).

Equation (10) has the same form as the Kirchhoff's first rule for solving electrical currents, which is not surprising since the equations governing the flow of electrical currents and hydraulic flow are identical. There is a one-to-one correspondence between the electrical current and the fluid volumetric flowrate, the voltage drop and the pressure difference, and the electrical resistance and the fluid resistance as defined in Equation (9). So the problem of solving for the fluid flow through a variable-aperture single fracture is equivalent to solving the electric current through a network of resistances. Figure 3c shows the electrical resistance analog of the fluid flow between adjacent nodes shown in Figure 3b.

Solute Transport

After the steady state fluid flowrates are obtained, the solute transport through the fracture is calculated using a particle-tracking technique (Schwartz et al., 1983; Robinson, 1984). A large number of particles are introduced in the known flow field at the fracture inlet (i.e., the left boundary of the square flow region as shown in Figure 3a). Particles coming to an intersection are distributed in the outlet branches (resistors) with a probability proportional to the flowrates (electrical current). Each particle is followed through the network of resistors. The residence time for the particle to traverse from one node to the next is determined by the flowrate between the adjacent nodes and the volume involved,

$$t_{ij}=\frac{\frac{1}{2}(b_i+b_j)\Delta x\Delta y}{nQ_{ij}} \tag{11}$$

where n is half the number of branches at each node. In our choice of square mesh, n equals 2. Summing the residence times t_{ij} traversed by the particle over the entire path from inlet to outlet (i.e., the right boundary of the square flow region in Figure 3a) gives the total residence time of the particle. In this calculation, we focus on the effects of the different residence times along the different pathways on the dispersion of tracer transport through the fracture. We therefore do not include the effects of molecular diffusion, matrix diffusion or local dispersion within each channel in our calculations.

RESULTS

Fluid Flow

Solutions of Equations (9) and (10) yield the pressure at each nodal point and the volumetric flowrate between adjacent nodes. The plots in Figures 4 and 5 correspond to the flowrates in the fractures with aperture variation as shown in Figures 1 and 2 respectively. Figures 4a through 4d display flowpaths for apertures with spatial correlation length 0.1, and Figures 5a through 5d are for cases with correlation length of 0.4. Hence the aperture variation in Figure 1a gives rise to the flowrate distribution displayed in Figure 4a, and that of Figure 2a gives rise to flowrates in Figure 5a, and so forth. The flowrates between the nodes vary over several orders of magnitudes, the large range of values arise from the fact that the local resistance to the fluid flow varies as the inverse of the local aperture raised to the third power, and the lognormal distribution of apertures originally assumed for the fracture plane already takes on a wide range of values. To display the variation of the large range of flowrates over the entire fracture, the volumetric flowrates are plotted in Figures 4 and 5, where the thickness of the lines joining nodes is made to vary as the square root of the flowrate; the thicker the lines, the larger the flowrates. The plots in Figures 4 and 5 show the following features. One, they all display the preferred paths of large volumetric flowrates that are formed because of the variation of the apertures within the single fracture plane. Two, the different spatial correlation of the variable apertures gives rise to different flow patterns. Figures 4a through 4d display flowpaths for apertures with spatial correlation length 0.1, and Figures 5a through 5d are for cases with correlation length of 0.4. We note that there is a tendency for all the flow paths of large flowrates to coalesce into a "channel" on the order of one spatial correlation length in width, and the spacing between these large flowrate "channels" also is on the order of the spatial correlation length of the fracture apertures.

Particle Tracking

Solute transport phenomena are investigated by tracking the particles advected through the fracture. Recall that the boundary conditions employed to solve the flow through the system is the constant head boundary condition, that is, all the nodes on the left hand boundary (Fig. 3a) are maintained at the higher pressure P_1, and all the nodes on the right boundary are maintained at the lower constant pressure P_2. Particles are let in at the left hand boundary and collected at the right hand boundary. A plot of the number of particles collected at all the outlets on the right hand boundary at different arrival times constitutes the breakthrough curve. Calculations have been carried out for total number of input particles ranging from several hundreds to 10000 in order to investigate the effect of the number of particles on the breakthrough curves. We found that calculations using 1000 particles are more than adequate since they already yield breakthrough curves that have very little spurious artifacts due to the finite number of particles employed. The breakthrough curves for total number of 1000 particles are indistinguishable from those with 10000 input particles.

Not only are we interested in the tracer breakthrough curves, but we are particularly interested in the manifestation of the channeling phenomena in tracer measurements. Therefore, in Figures 6 and 7 we present the spatial distribution of the tracer collection in the outlets. The horizontal x-axis corresponds to the spatial axis of the right (exit) boundary in Figure 3a. The origin on the horizontal axis in Figures 6 and 7 corresponds to the bottom right corner of the flow region in Figure 3a; and x=1.0 corresponds to the top right corner of the flow region. The vertical axis in Figures 6 and 7 gives the number of particles collected at the exit co-ordinates. The results are shown for a total number of 2000 input particles. Note the patterns of the histograms in Figures 6 and 7 and, in particular, the relationship of their shapes with the different spatial correlation lengths of the fracture apertures which are 0.1 and 0.4 respectively. We can perhaps see a trend of the tracer concentration distributed spatially in "channels" of spatial width on the order of a spatial correlation length and spaced also on the order of one correlation length.

In general, the breakthrough curves of tracer transport in two dimensions through these variable-aperture fractures have a fast rise at early times, since the majority of particles take the fast flow paths; then there is a long tail in the breakthrough curve due to a small fraction of particles meandering through the fracture, including in their flowpaths many sections with extremely small volumetric flowrates. To see the tracer breakthrough characteristics as a function both of time and space, we did the following. The times at which 25%, 50%, 75%, and 100% of the particles have arrived at the exit boundary are denoted respectively by $t_{0.25}$, $t_{0.5}$, $t_{0.75}$, and $t_{1.0}$. Figures 8a through 8d show the spatial distribution of particles collected at times $t_{0.25}$, $t_{0.5}$, $t_{0.75}$ and $t_{1.0}$ respectively. Each figure is a contour plot of the number of particles. The x axis represents the spatial axis of the left hand boundary in Figure 3a, which is the boundary for inlets. The y axis represents the spatial axis of the right hand boundary, which is the boundary for outlets. In experimental measurements, information as to the position of the outcoming tracer at different times can be gathered; hence the y coordinate of the tracer concentration in Figure 8 correspond to the kind of data that may be collected if channeling phenomena are present. On the other hand, the position from which the outcoming tracer originates is contained in the x coordinates in Figure 8; this information can be obtained experimentally only when different tracers (e.g., different dyes) are introduced at different locations at the input boundary. The contours denote the particle number densities that enter or exit the single fracture. Contour curves of the same nature as Figure 8, but only at $t_{1.0}$ are displayed in Figures 9 through 11 for different realizations of spatial aperture distribution. We have labeled this kind of plot as "transfer matrix", since it contains the information involving the transfer of particles from the entrance boundary to the exit boundary. Figures 8 and 9 are contour plots of the transfer matrix for two different realizations of aperture variation with the spatial correlation 0.1, and Figures 10 and 11 are for realizations with the spatial correlation 0.4 of the linear dimension of the flow region. The contours in Figures 8, 9, 10 and 11 are derived from the aperture distribution as shown in Figures 1c, 1d, 2b, and 2d respectively. The channeling phenomenon of tracer transport in a single fracture with variable apertures is well demonstrated in these figures: the fast flow paths for tracer transport tend to coalesce

into "channels" with width and spacing on the order of one spatial correlation length. A comparison of Figures 8 and 9 with figures 10 and 11 clearly shows the difference between the cases with correlation 0.1 and 0.4. This kind of plots of measurable data may be a means to estimate the spatial correlation lengths of the system.

Figures 12 and 13 show the percentage of the particle breakthrough along the exit line as a function of time normalized to the mean residence time, t_m, for four realizations of spatial correlation 0.1 and 0.4 respectively. Here t_m is calculated by taking the average of all the residence times of the 2000 particles. It is interesting to note that firstly the different realizations give similar values within a narrow band, and secondly the results for spatial correlation of 0.1 and 0.4 are similar, so that one may suggest that such a plot is insensitive to the spatial correlation length.

INTERPRETATION OF 2-D RESULTS BY THE 1-D CHANNEL MODEL

It is of interest to know the aperture values along the flow paths actually taken by each of the particles. Our calculation involved tracking 400 particles through the single fracture, grouping them in quadrants according to their residence times within the fracture. Statistical analysis were done on the apertures along the actual flow paths. The mean and standard deviation on the logarithm of the apertures were computed. Calculations were carried out for all eight realizations of the single fracture (Figs. 1 and 2) and the results are tabulated in Tables 1 and 2. Although all eight realizations were generated with the same aperture density parameters (mean, $\log b_o$=1.7, and standard deviation, σ=0.43), Table 1 shows that mean and standard deviation of actual log aperture values in the fracture for these realizations can be quite different from each other. It also show that apertures along the particle flow paths take on a larger mean and smaller standard deviation than the apertures over the whole fracture. We note that the distinction between the "fast" and "slow" particles is that the variance of the aperture distributions of the actual flow paths taken by the particles seem to increase for the "slower" particles. The larger variance implies that a larger range of apertures, both large and small, are present along the particle flow paths. However, it is the occurrence of the small apertures that gives rise to the large residence times and makes the particles

"slow." Although the fastest particles have the largest mean and smallest standard deviation, the variation of the mean and standard deviation among the quadrants are not large, and the values in Tables 1 and 2 indicate that average values of the mean and standard deviation can be used to characterize the log apertures along the flow paths of all the particles, be they slow or fast. We also calculated the aperture density distributions for the flow paths and for the fracture, for the eight realizations. Figures 14 and 15 show typical normalized aperture density distributions for the fracture (broken curve), and for the particle flow paths (solid curve). These figures illustrate clearly that the smallest apertures are avoided in two-dimensional flow through a fracture. However, it is also important to note that the particles cannot avoid the small apertures entirely.

In our earlier work (Tsang and Tsang, 1987), we used a system of one dimensional channels, statistically generated with a given aperture distribution and a spatial correlation length, to interpret the fluid flow and solute transport in two- and three-dimensions. We apply the methodology outlined there, employing a lognormal aperture distribution with parameters for the actual particle paths as given in Tables 1 and 2 to generate a system of one dimensional channels. The tracer concentration transport as a function of time, assuming a step function tracer input are plotted in Figure 16 for the fractures corresponding to Figures 1 and 2. Only 7 realizations are plotted, with the omission of the case shown in Figure 2b, where the channel is too close to the upper no-flow boundary, resulting in an aberration of the aperture density function. When Figure 16 is compared with Figures 12 and 13, which show breakthrough curves derived from particle tracking in two-dimension, it is found that the breakthrough curves shown in Figure 16 from the one-dimensional calculation fall within the same range as those from two-dimensional calculations in Figures 12 and 13. Furthermore, the shape of the breakthrough curves are also similar, with fast rise at early times and a rather long tail. To facilitate the comparison between the one-dimensional and two-dimensional calculations we plot them together in Figure 17. The filled dots are results for the averages of the two-dimensional calculations for the seven realizations. The open circles are the averages of the one-dimensional channel model calculations using the aperture density distributions given in Tables 1 and 2. The vertical bars give the limits of the spread of the

values of the seven realizations. The agreement between the one- and two-dimensional calculations is good. Since this kind of plot is a measure of dispersivity of tracer transport through the fracture, our results seem to indicate that the variable-aperture, one-dimensional channel model can reproduce the two-dimensional tracer transport dispersivity.

We also took the aperture density distribution from Tables 1 and 2 and constructed a system of constant-aperture channels and computed the breakthrough. This is the traditional bundle of flowtubes channel model (for example, Neretnieks,1983). The results are shown as open squares in Figure 17. Finally if the entire fracture has only one constant aperture, then the plot in Figure 17 would be a step with tracer concentration equals 0 before $t/t_m = 1$ and 100% after, implying a piston flow with zero dispersivity. The results for the tracer breakthrough through such a parallel plate representation of a single fracture are shown as open triangle in the figure.

Table 3 presents the mean residence times from the different calculations for a number of realizations. The second column gives the expected values obtained by dividing total fracture aperture volumes by the calculated mean flowrates in two dimensions. The third column gives the mean particle residence times from the breakthrough curves derived from particle tracking in two dimensions. These agree within a few percent of the values in column 2. The fourth column gives the mean residence times from the breakthrough curves derived from the one-dimensional variable aperture channel model. we note that the mean residence times are within factor of 2 as those derived from the actual two-dimensional transport. The last column gives the mean residence times obtained from the breakthrough curves derived from a system of constant-aperture channels. The mean residence times in this last column are typically two or three orders of magnitude smaller than that predicted from both the two-dimensional and one-dimensional variable aperture channel calculations. This is easy to understand since in the constant aperture channel representation, the larger the aperture, the shorter the residence time, therefore the average is heavily weighted by the residence times of the largest constant aperture channels.

DISCUSSIONS

Flow in Single Fractures

The calculated flow patterns shown in the previous section bear strong resemblance to field observations made on a single fracture by Bourke (1987). Packer tests were carried out in a single granitic fracture with dimensions of about 2 m in a Cornwall quarry. Five boreholes are drilled in the plane of the fracture. By packing off 8 cm sections of each borehole, pressure interference tests between adjacent boreholes were performed. Based on observed communication between different sections of the five boreholes, it was deduced that there is strong flow channeling in the single fracture (Figure 18). Two major flow channels were observed, with only about 10-20% of the fracture plane participating in the flow. This observation can be understood in terms of our model.

Pyrak-Nolte et al. (1987) studied apertures of a single fractures in 5.2-cm core samples in the laboratory. They injected molten Wood's metal into the single fracture and let it solidify, then they opened up the fractures and examine the two fracture surfaces using a scanning electron microscope. Composites from SEM micrographs of fracture surfaces allow identification of the areas that are open to flow, as indicated by white areas in Figure 19. The black shading in Figure 19 indicates contact areas with zero fracture aperture. Note the resemblance of the general character of Figure 19 to that of Figure 2, where we show statistically generated variable apertures in a single fracture, with spatial correlation length of 0.4. One feature in Figure 19 is the "pools" of open apertures (white areas) available for fluid flow. However, the open areas only indicate that the apertures are non-zero, they contain no information as to the magnitude of the apertures, and hence the large "pools" in Figure 19 do not necessarily imply areas of uniformly large flow rate. On the other hand, Figure 2 does contain information on the magnitudes of the apertures and thus fluid flow may be derived as shown in Figure 5. In our model, these "pools" of open apertures observed experimentally (Fig. 19) results in a localized group of intersected flow paths (Fig. 20a). Such patterns are typically found in Figures 4 and 5. Such a situation as shown in Figure 20a can also be represented by flow along streamlines through the pools as shown in Figure 20b. In Figure 20b, the

longer the streamlines, the slower are their flow velocities, and the flow velocity is never zero. However, if the velocity in the pool is very small, then the pool becomes essentially a static reservoir of water, whose main role is not to provide streamline paths, but to exchange solute with the major flow line by diffusion (Fig. 20c). These "stagnant pools" were proposed by Neretnieks (1985). Our present calculation does not take account of the process represented in Figure 20c.

Now let us compare exit tracer mass flowrates for spatial correlation, λ equals 0.1 (Fig. 6) and those for λ equal to 0.4 (Fig. 7). The spacings between locations of maximum mass flowrate and between locations of zero mass flowrate appear to bear a relationship with the spatial correlation of the variable apertures in a single fracture. Hence to obtain a crude estimate of the correlation length one may monitor the spacings of tracer exit points along a fracture trace in the ceiling or wall of a drift. a drift. However, the duration of the experiment should be long enough for exit concentrations to reaching a stationary value or a value comparable to the inlet concentration. The transfer matrix patterns (Fig. 8-11) also suggest that useful information such as the relevant spatial correlation length which governs the spacing of flow channels may be obtained from experimental setup which aims at "line measurements" rather that "point measurements". The transfer matrix may be constructed if experiments are performed with a line of input points on the high-pressure side of the single fracture and a line of observation points on the opposite low-pressure side. Different tracers are then injected at different points in packed-off sections along the input line, and long-term tracer observations are made along the exit line.

It is also of interest to measure and compare the distribution of fluid flowrates with that of tracer mass flowrates along an exit line, when tracer is released at one point on the high- pressure input line. Generally they are not the same. Our calculation for the fracture with the aperture variation of Figure 1a gives results as shown in Figure 21. The calculation is for tracer released at only one location (y=.77) on the entry line of the fracture. In Figure 21, the unfilled bars denote the relative fluid flowrates along the exit line, and the filled bars give the relative mass flowrates. Abelin et al. (1985) monitored fluid and tracer arrivals along a single fracture trace in the ceiling of a drift in the

Stripa mine. The collection points of fluid and tracer were placed at 0.7m interval. Tracer was injected through a bore hole into the single fracture at a point about 5m above the drift ceiling. It was found that both fluid and tracer emerged only at a few spots along the fracture trace, with about 90% of the flowrate carried by less than 20 % of the 0.7m observation sections. Furthermore, at a number of observation point where large fluid flowrate were obtained, no tracer was observed. If the tracer had been released all along the input line, the fluid flow exit distribution will be similar to tracer exit distribution after a time period much longer than the tracer mean residence time. In this regard it may be suggested that the fluid flow exit patterns may be more useful in determining fracture spatial correlation lengths which controls the flow pattern when channeling is present.

We would like to make some general remarks in the "relevant" spatial correlation length that controls the channeling flow pattern. The two-dimensional calculations presented above show that the spatial correlation of the apertures controls the width and spacing of the flow channels. If the spatial correlation length is very small compared to the dimension of the flow region at which measurements are taken, channeling phenomena should disappear and porous medium behavior should prevail. The fact that there exist experimental evidences of flow channeling in scales ranging from centimeters in the laboratory to meters and tens of meters in the field suggests to us that at different scales of measurement, the "relevent" spatial correlation length that governs the channeling flow pattern is on the same order of magnitude as the measurement scale. In other words, if the aperture variation in a single fracture were a fractal (Wang and Narasimhan, 1987; Brown, 1987), then at larger and larger measuring scale, larger and larger irregularity is encountered, and it is the largest possible irregularities on the scale of measurement that control the flow pattern.

Implications of Results on Flow in Multi-Fracture Systems

In our earlier work (Tsang and Tsang, 1987), we hypothesized that the flow in single fractures and the flow in intersecting multi-fracture systems may be analyzed on the same basis; i.e., as flow along one-dimensional channels of variable aperture. From the

discussions above, we demonstrated (Fig. 17 and Tables 1 through 3) that the flow and tracer transport in two-dimensional single fracture can be represented by transport through variable-aperture, one-dimensional channels for the cases considered.

For the multi-fractured systems, the channel width is still expected to be of the order of the aperture correlation length in the single fracture. Spacing between channels, on the other hand, would depend more on fracture spacings and characteristics of different fracture sets. Thus it is expected to be much larger, of the order of fracture spacings. In the case of very tight systems where many of the fractures are not hydraulically conducting, the channel spacing should be even larger, of the order of the spacing of conducting fractures. The spacing of these conducting channels defines the effective spatial correlation length for flow and transport in three dimensions.

With the above comment on the effective correlation length, many of the results and discussions on single fractures in previous sections are directly applicable to the multi-fracture media. Thus the usefulness and importance of making tracer measurements with line tracer injection and line or areal observation of tracer emergence is obvious. This kind of measurements should enable one to make transfer matrix plots and may give an indication of the effective correlation length. If channeling is of primary importance in a particular flow system, then the spacing between conducting channels, which is related to the effective correlation length, is a key parameter. This information cannot be obtained by point measurements readily. Hence areal or line fluid flow and tracer emergence measurements with a number of injection points with different tracers will be very relevant.

ACKNOWLEDGMENTS

The review and comments by Drs. Karsten Pruess and T. N. Narasimhan are much appreciated. This work was supported through U.S. Department of Energy contract DE-AC03-76SF00098 by the Assistant Secretary for Energy Research, Office of Basic Energy Sciences, Division of Engineering and Geosciences, and by the Office of Civilian Radioactive Waste Management, Office of Geologic Repositories, Engineering and Geotechnology Division.

REFERENCES

Abelin, H. J. Gidlund, and I. Neretnieks, Migration Experiments in a Single Fracture in the Stripa Granite: Preliminary Results, in Proceedings of the Workshop on Geological Disposal of Radioactive Waste In Situ Experiments in Granite, Stockholm, Sweden, pp. 154-163, Organization for Economic Co-Operation and Development, Paris, 1983.

Abelin, H., I. Neretnieks, S. Tunbrant and L. Moreno, Final Report on the Migration in a Single Fracture, Experimental Results and Evaluation, Sven. Kärnbränsleförsorjning Tech. Rep. 85-03, Nuclear Fuel Safety Project, Stockholm, 1985.

Bianchi, L., and D. Snow, Permeability of Crystalline Rock Interpreted from Measured Orientations and Apertures of Fractures, *Ann. Arid Zone,* Vol. 8, No. 2, p. 231-245, 1968.

Bourke, P. J., Channeling of Flow through Fractures in Rock, Proceedings of GEOVAL-87 International Symposium, Stockholm, Sweden, April 7-9, 1987.

Bourke, P. J., E. M. Dunance, M. J. Heath and D. P. Hodgkinson, Fracture Hydrology Relevant to Radionuclide Transport, Rep. 11414, Atomic Energy Research Establishment, Harwell, United Kingdom, 1985.

Brown, S. R., Fluid Flow through Rock Joints: The Effect of Surface Roughness, *Jour. Geophys. Res,* Vol. 92, B2, p. 1337-1347, 1987.

Gentier, S., Morphologie et Comportment Hydrom'ecanique d'une Fracture Naturelle dans un Granite Sours Contrainte Normale, Doctoral Thesis, U. d'Orl'eans, France, 1986.

Narasimhan, T. N., Geometry - imbedded Darcy's Law and Transient Subsurface Flow, *Water Resources Research,* Vol. 21, No. 8, pp. 1285-1292, 1985.

Neretnieks, I., A Note on Fracture Flow Dispersion Mechanisms in the Ground, *Water Resources Research,* Vol. 19, No. 2, pp. 364-370, 1983.

Neretnieks, I., Transport in Fractured Rocks, in Proceedings, Memoirs of the 17th International Congress of International Association of Hydrologists, Vol. XVII, pp. 301-318, International Association of Hydrologists, Tucson, AZ, 1985.

Pyrak-Nolte, L. J., L. R. Myer, N. G. W. Cook and P. A. Witherspoon, Hydraulic and Mechanical Properties of Natural Fracture in Low Permeability Rock, to appear in Proceedings of Sixth International Rock Mechanics Symposium, Montreal,

Canada, 1987.

Pyrak, L. R., and L. R. Myer, and N. G. W. Cook, Determination of Fracture Void Geometry and Contact Area at Different Effective Stress, EOS Trans. AGU (abstract), Vol. 66, No. 46, 903 p, 1985.

Robinson, P., Connectivity, Flow and Transport in Network Models of Fractured Media, Ph.D. thesis, Oxford University, Report TP.1072 Theoretical Physics Division, AERE Harwell, Oxfordshire, England, 1984.

Schwartz, F. W., L. Smith and A. S. Crowe, A Stochastic Analysis of Macroscopic Dispersion in Fracture Media, *Water Resources Research,* Vol. 19, No. 5, pp. 1253-1265, 1983.

Tsang, Y. W. and C. F. Tsang, Channel Model of Flow through Fractured Media, *Water Resources Research,* Vol. 23, No. 3, pp. 467-479, 1987.

Tsang, Y. W., C. F. Tsang, and I. Neretnieks, Some Properties of a Channeling Model of Fracture Flow, Sven. Karnbränsleförsorjning Technical Report, Nuclear Fuel Safety Project, Stockholm, in press, 1987.

Wang, J. S. Y. and T. N. Narasimhan, Aperture Correlation of Fractal Fracture, submitted to Water Resources Research, 1987.

Williams, S. A. and A. I. El-Kadi, Covar - A Computer Program for Generating Two-Dimensional Fields of Autocorrelated Parameters by Matrix Decomposition, International Groundwater Modeling Center, Holcomb Research Institute, Butler University, Indianapolis, ID, 1986.

Table 1. Statistics for apertures along actual particle paths, and for the entire fracture of Figures 1a-d.

Correlation $\lambda = 0.1$	Realization 511		Realization 512	
	Mean ($\log b_0$)	Standard Dev. (σ)	Mean ($\log b_0$)	Standard Dev. (σ)
Fracture Aperture	1.74	0.41	1.59	0.46
Fastest 25% particles	2.03	0.34	1.89	0.33
Second 25% particles	2.00	0.36	1.90	0.37
Third 25% particles	1.99	0.38	1.89	0.36
Slowest 25% particles	1.97	0.39	1.84	0.43
All particles	2.00	0.37	1.88	0.38

Correlation $\lambda = 0.1$	Realization 513		Realization 514	
	Mean ($\log b_0$)	Standard Dev. (σ)	Mean ($\log b_0$)	Standard Dev. (σ)
Fracture Aperture	1.76	0.42	1.75	0.43
Fastest 25% particles	2.09	0.29	2.17	0.28
Second 25% particles	2.06	0.30	2.14	0.30
Third 25% particles	2.02	0.32	2.03	0.35
Slowest 25% particles	1.98	0.36	1.94	0.37
All particles	2.04	0.32	2.07	0.34

Table 2. Statistics for apertures along actual particle paths, and for the entire fracture of Figures 2a-d.

Correlation $\lambda = 0.4$	Realization 541		Realization 542	
	Mean (log b_0)	Standard Dev. (σ)	Mean (log b_0)	Standard Dev. (σ)
Fracture Aperture	2.11	0.38	1.38	0.41
Fastest 25% particles	2.43	0.32	1.86	0.41
Second 25% particles	2.43	0.31	1.89	0.42
Third 25% particles	2.36	0.29	1.81	0.42
Slowest 25% particles	2.33	0.34	1.61	0.43
All particles	2.39	0.32	1.79	0.43

Correlation $\lambda = 0.4$	Realization 543		Realization 544	
	Mean (log b_0)	Standard Dev. (σ)	Mean (log b_0)	Standard Dev. (σ)
Fracture Aperture	1.45	0.38	1.70	0.43
Fastest 25% particles	1.95	0.34	2.12	0.33
Second 25% particles	1.93	0.35	2.15	0.33
Third 25% particles	1.86	0.35	2.13	0.36
Slowest 25% particles	1.68	0.39	2.04	0.38
All particles	1.85	0.38	2.11	0.36

Table 3. Mean residence times calculated from (a) mean fracture volume divided by mean calculated flow rates, (b) mean article travel times from 2-D calculations, (c) mean residence times from a system of statistically equivalent 1-D variable-aperture channels and (d) mean residence times from a system of constant-aperture channels.

Run	Mean Residence Time			
	Expected	Variable 2-D	Constant Aperture Channel	Aperture Aperture Channel
511	0.58	0.57	0.82	0.004
512	1.42	1.38	1.64	0.012
513	0.34	0.33	0.39	0.007
514	0.32	0.30	0.41	0.006
541	0.07	0.07	0.06	0.0005
542	2.23	2.23	3.10	0.007
543	0.84	0.85	1.15	0.0047
544	0.30	0.30	0.35	0.003

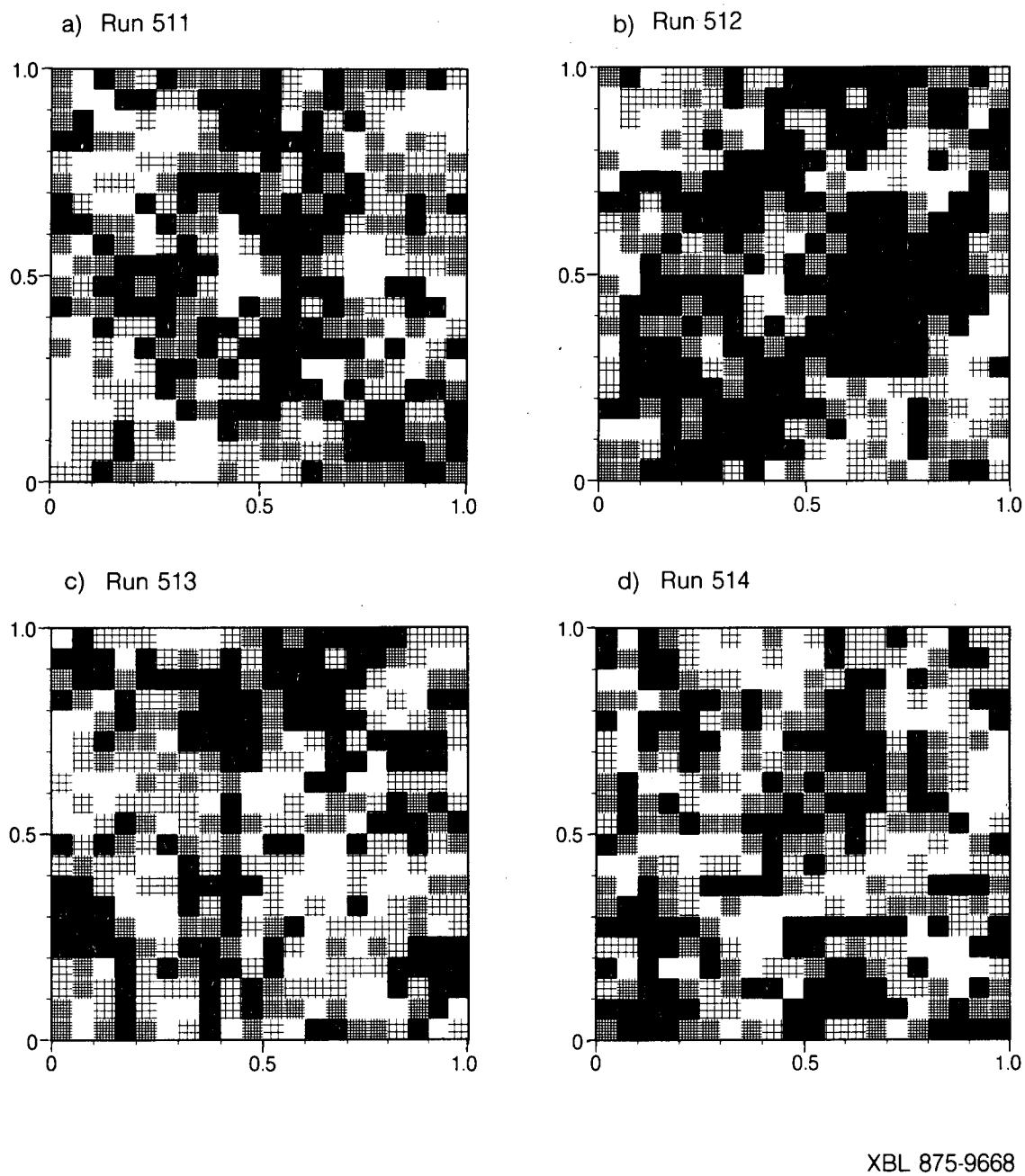

Figure 1a-d. Statistically generated apertures with a spatial correlation length of 0.1 in the plane of a single fracture of linear dimension 1.0.

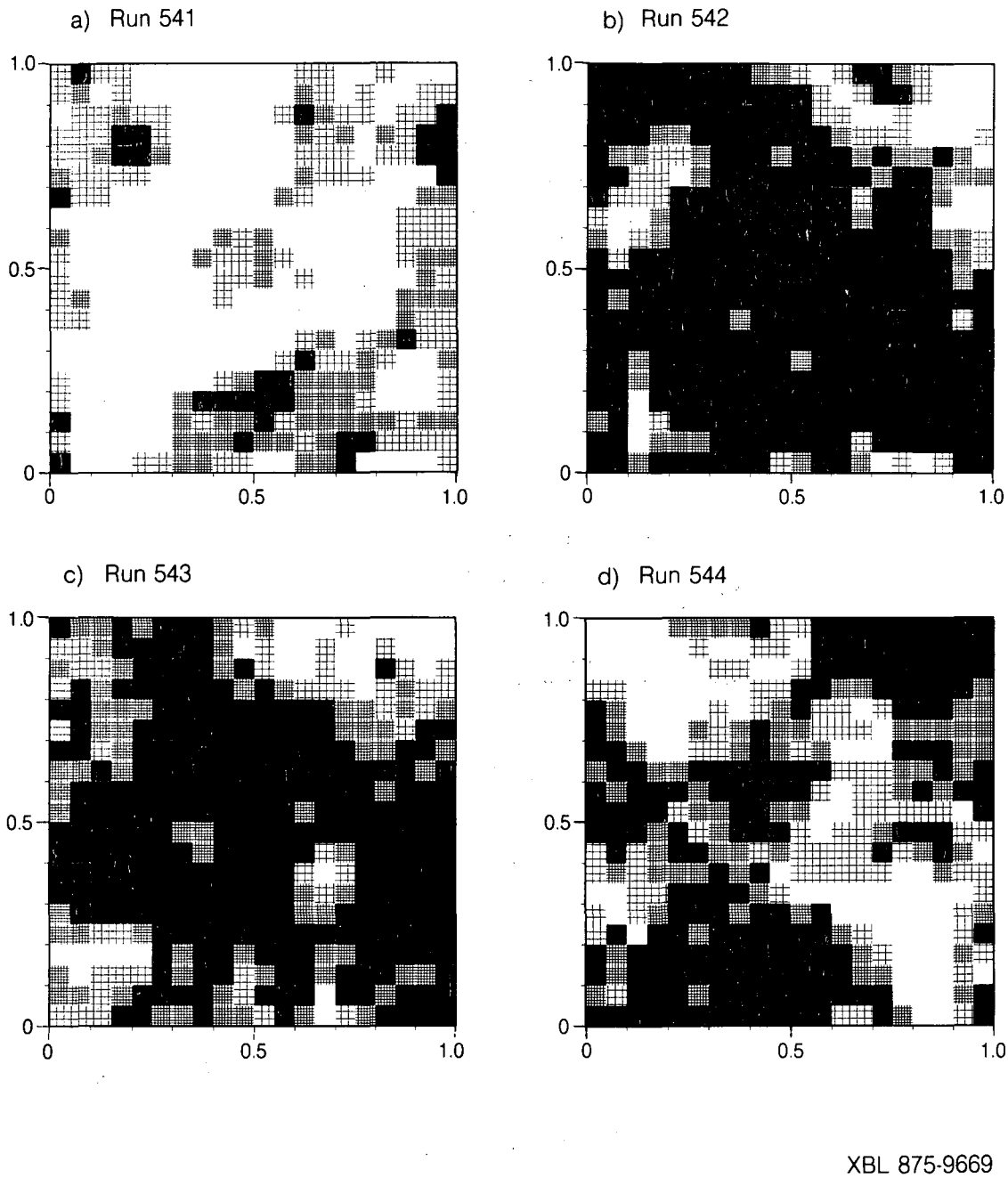

Figure 2a-d. Statistically generated apertures with a spatial correlation length of 0.4 in the plane of a single fracture of linear dimension 1.0.

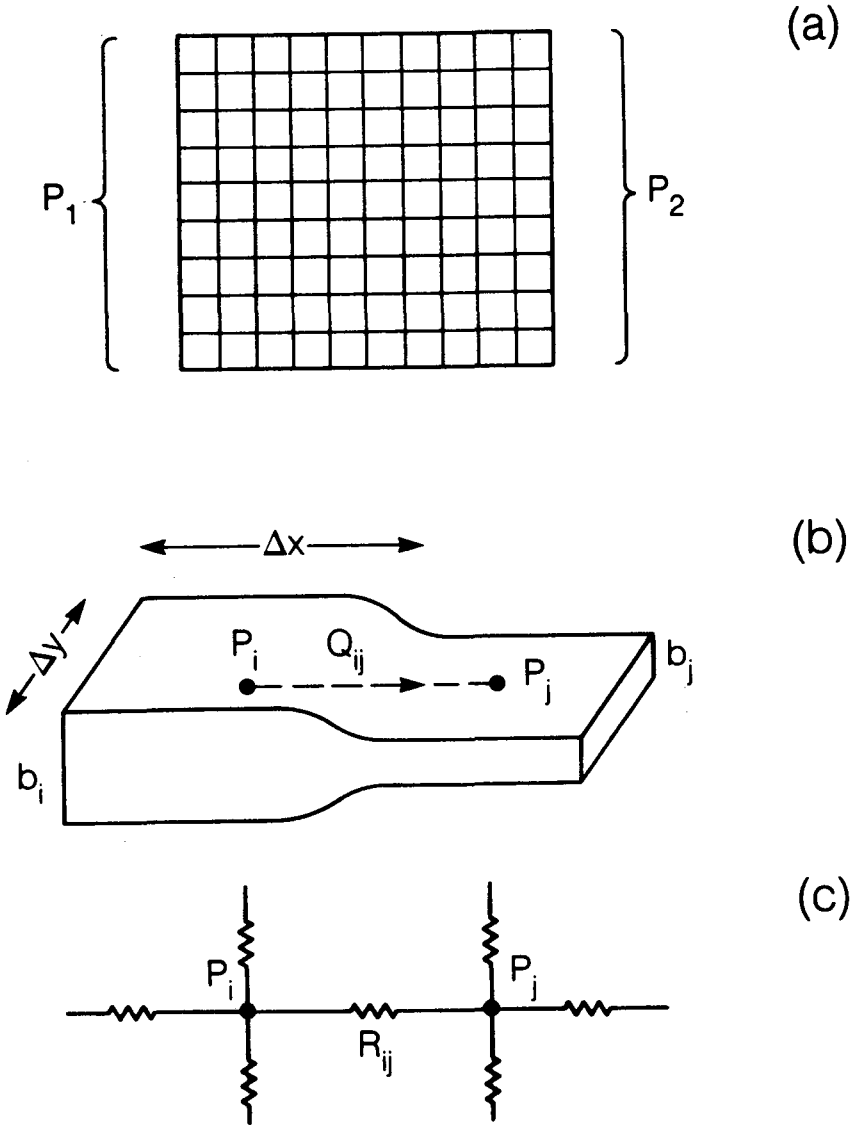

$$R_{ij} = 6\mu \frac{\Delta x}{\Delta y} \left(\frac{1}{b_i^3} + \frac{1}{b_j^3} \right)$$

XBL 873-10019

Figure 3. (a) Schematic diagram for flow through a single fracture with different aperture values assigned to areas bounded by grid lines.
(b) Schematic diagram for two adjacent nodes of different apertures: b_i and b_j and the fluid flow Q_{ij} between them.
(c) Electric analog of fluid flow between adjacent nodes.

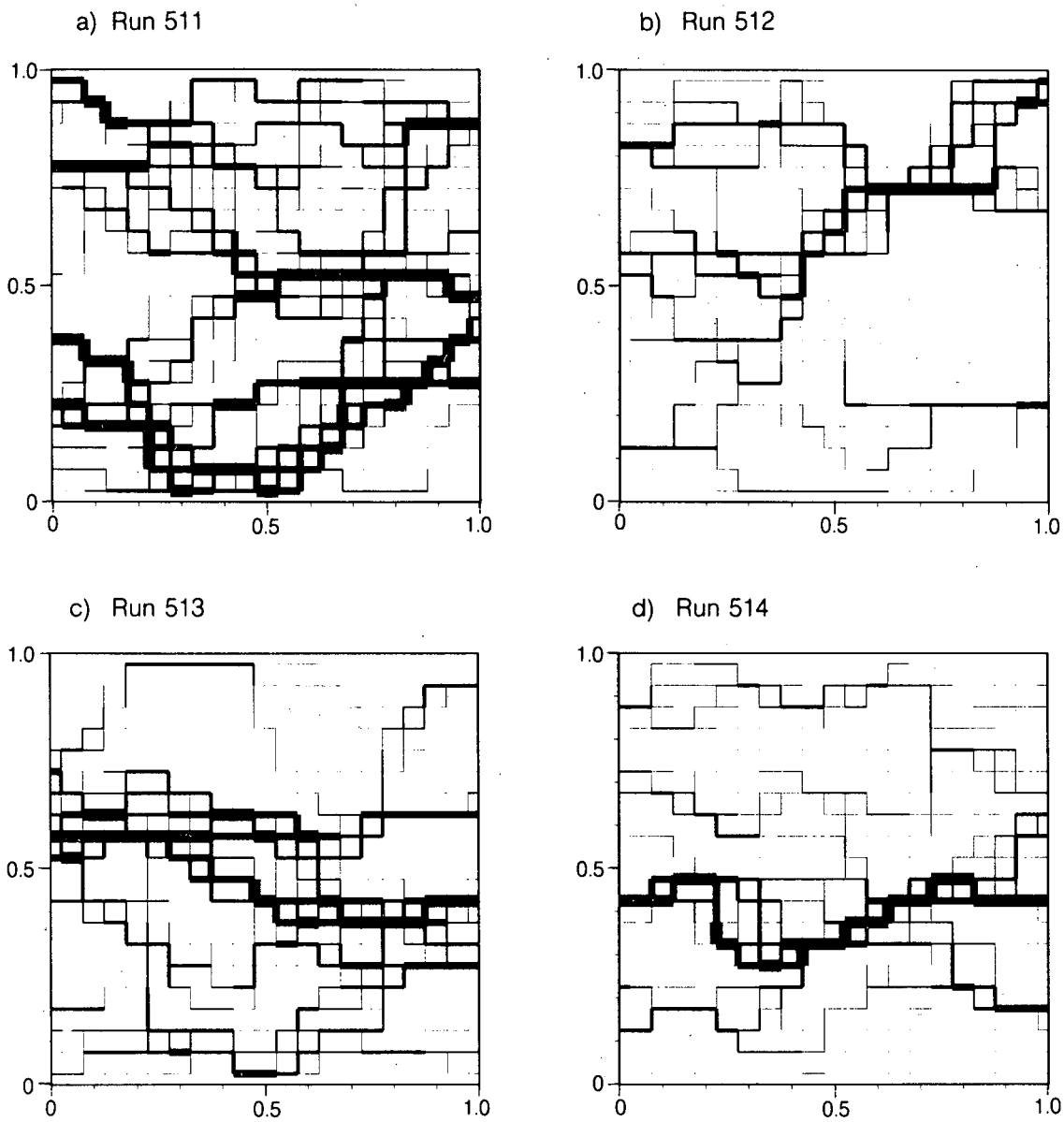

XBL 875-9670

Figure 4a-d. Fluid flow rates for the fractures with aperture variation as shown in Figure 1. The thickness of the lines is proportional to the square root of the flowrate.

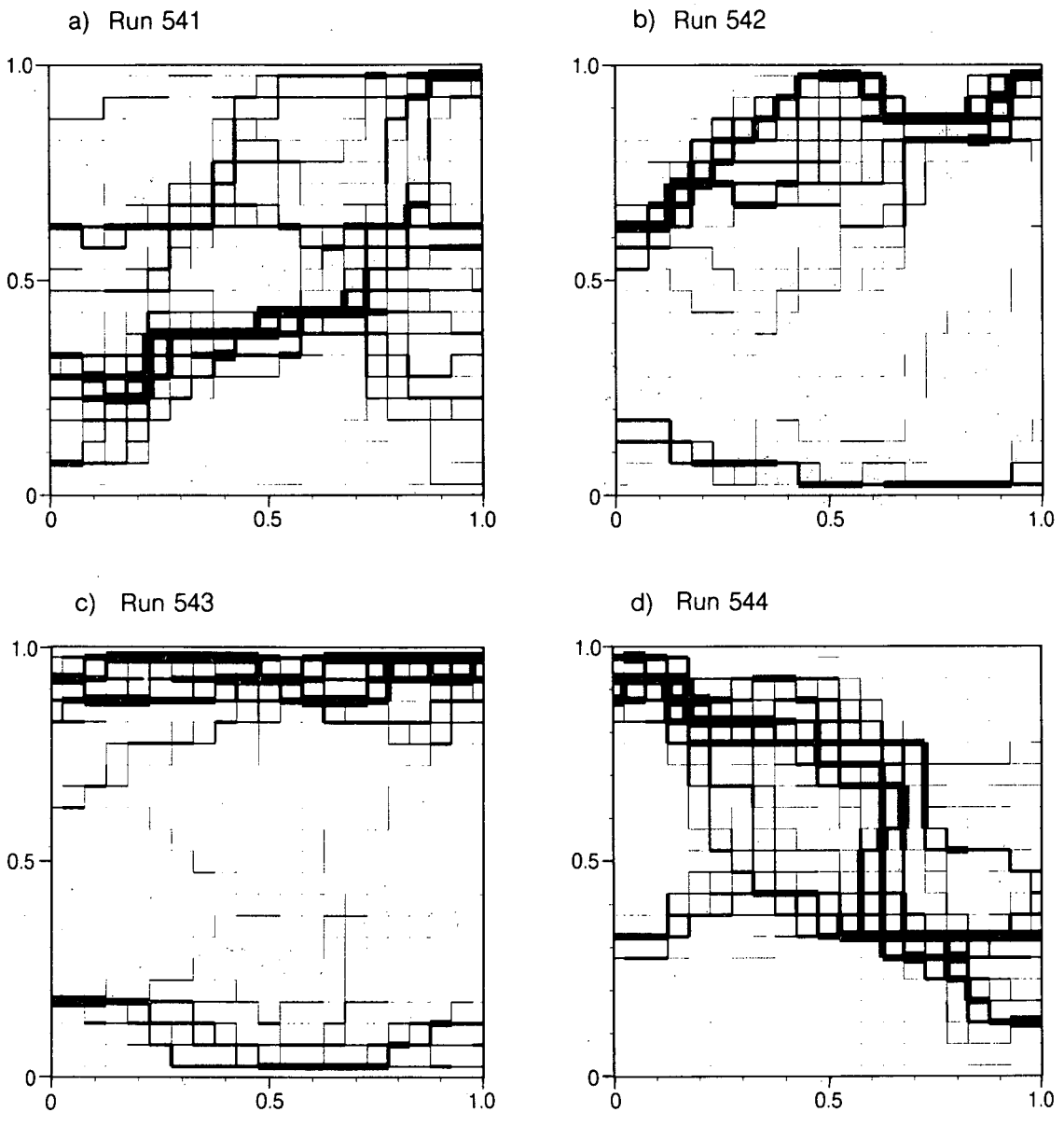

XBL 875-9671

Figure 5a-d. Fluid flow rates for the fractures with aperture variation as shown in Figure 2. The thickness of the lines is proportional to the square root of the flowrate.

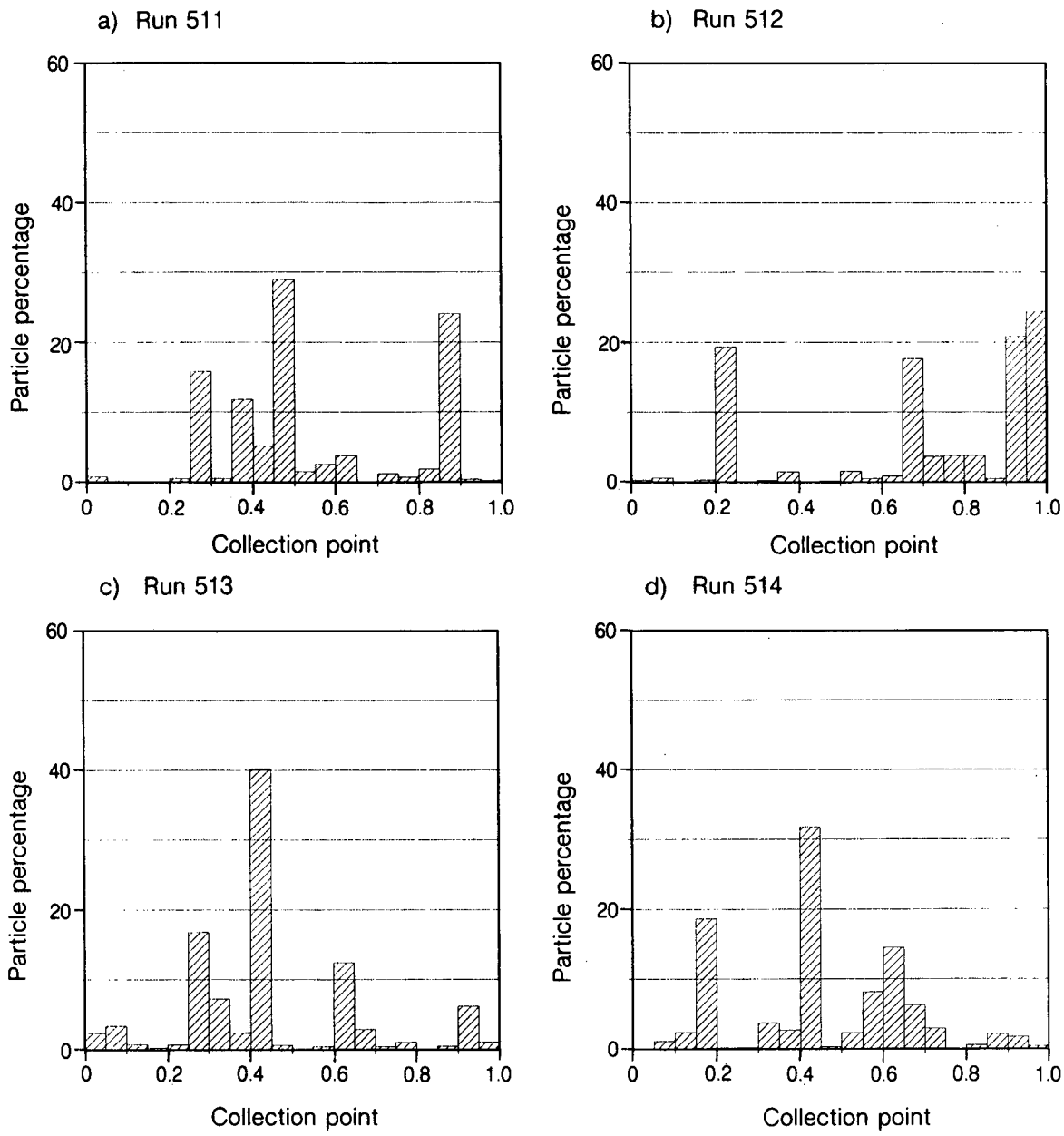

XBL 875-9672

Figure 6. Histograms of particle number as a function of position on the collection line, for fractures with spatial correlation length of 0.1.

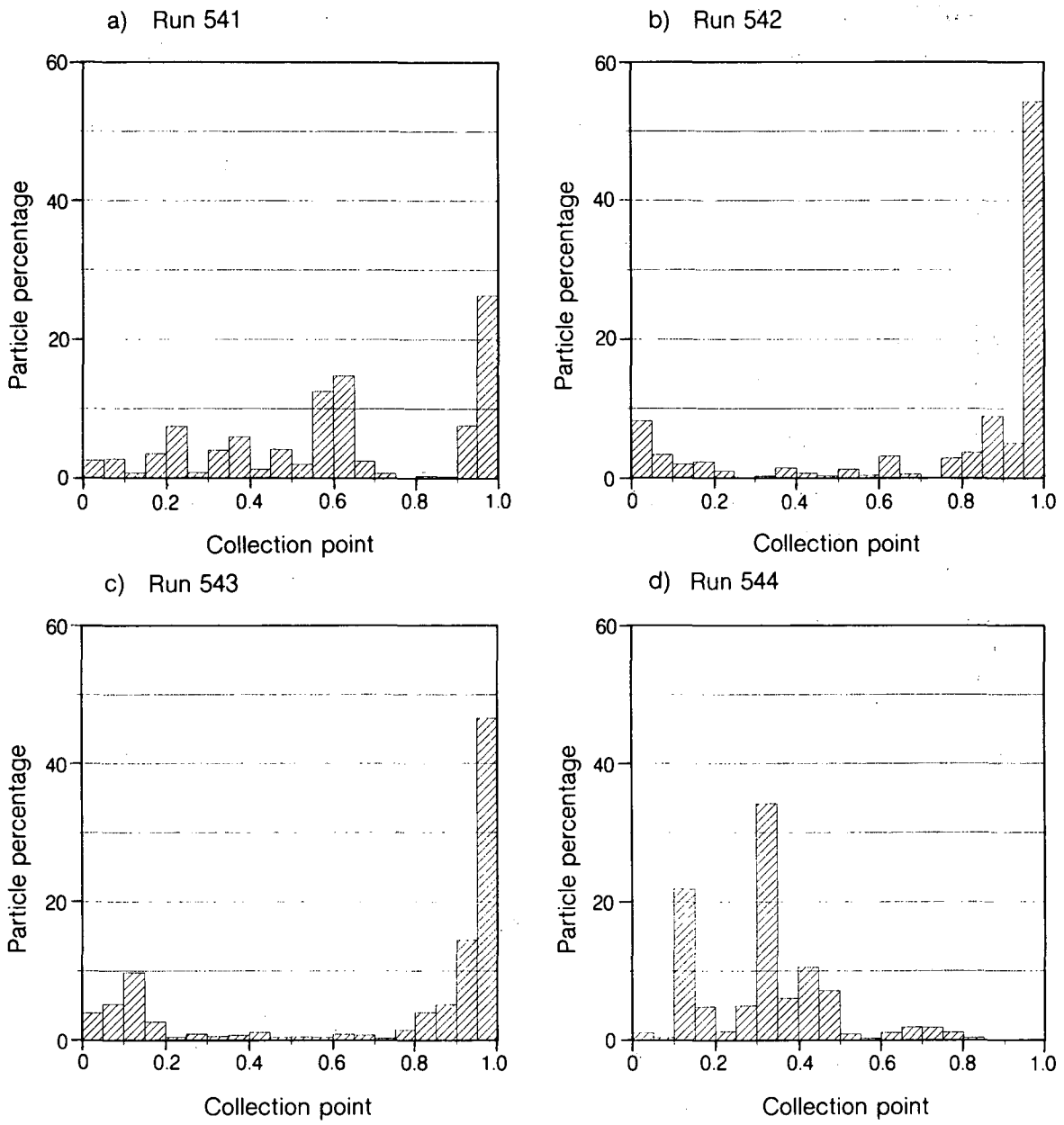

XBL 875-9673

Figure 7. Histograms of particle number as a function of position on the collection line, for fractures with spatial correlation length of 0.4.

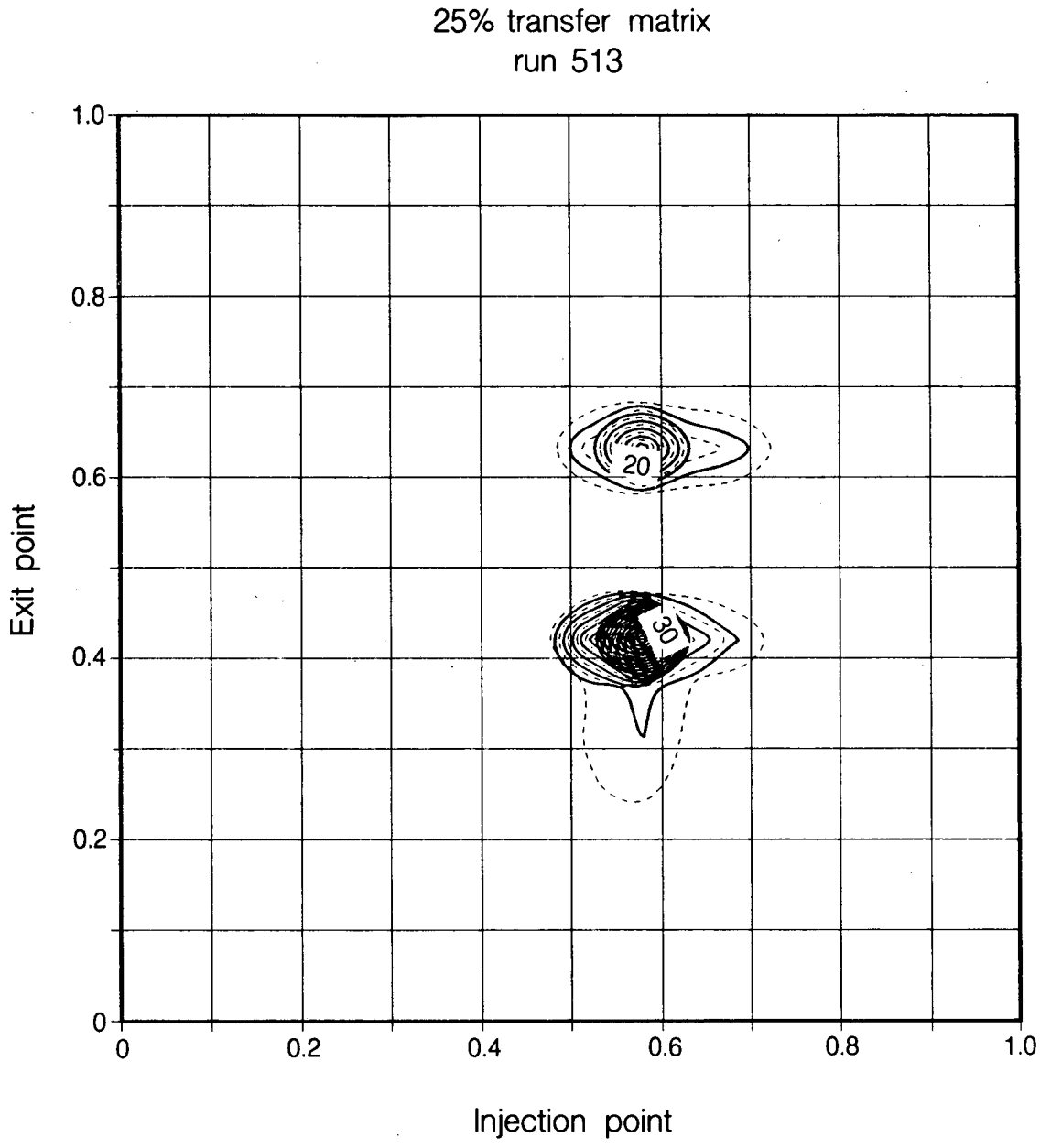

XBL 875-9674

Figure 8a. Contours of particle number density as a function of tracer entrance location and collection location, for a fracture with aperture variation as shown in Figure 1c at $t_{.25}$, when 25 % of the input particles have arrived at the exit boundary.

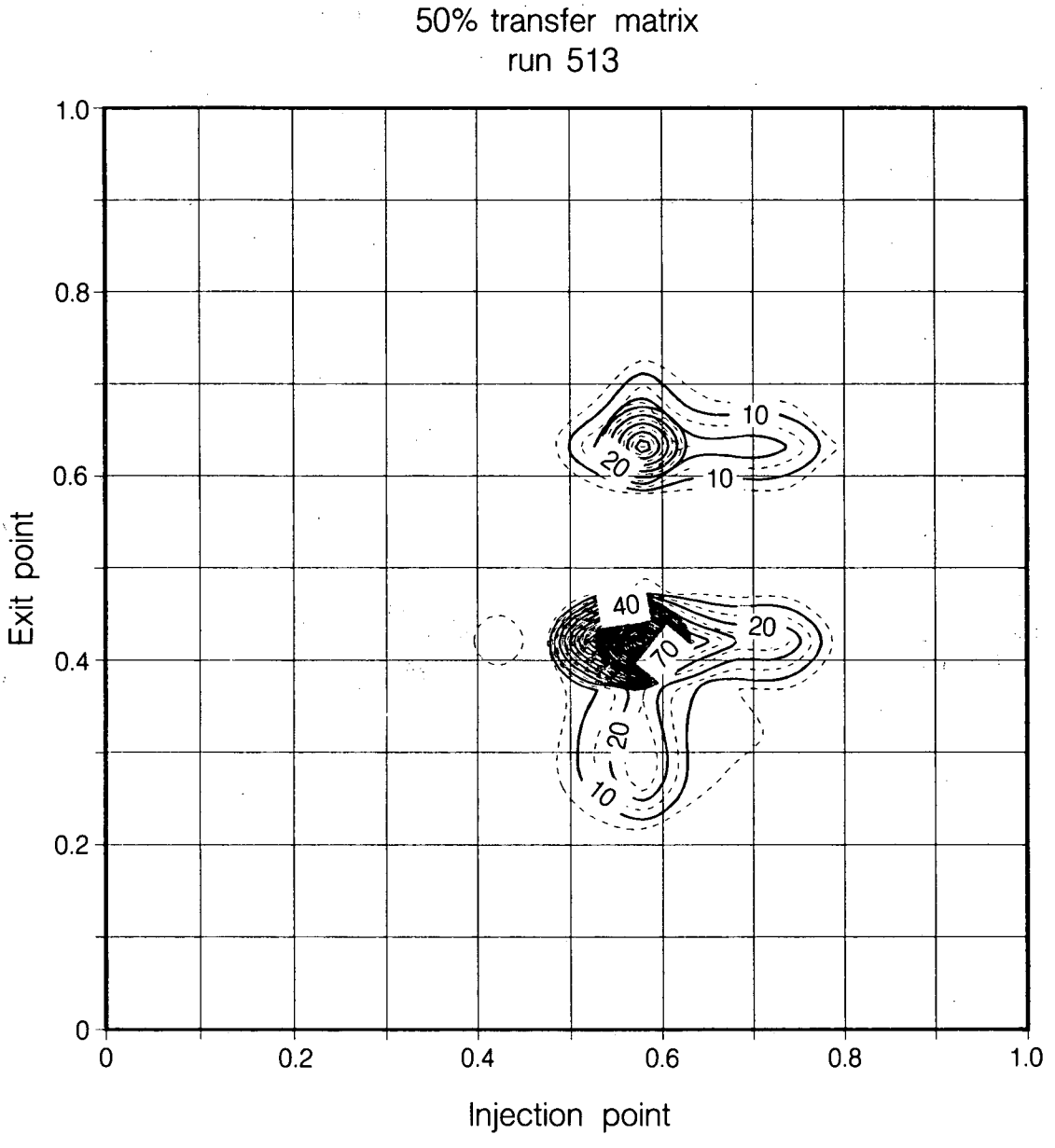

XBL 875-9675

Figure 8b. Contours of particle number density as a function of tracer entrance location and collection location, for a fracture with aperture variation as shown in Figure 1c at $t_{0.5}$, when 50 % of the input particles have arrived at the exit boundary.

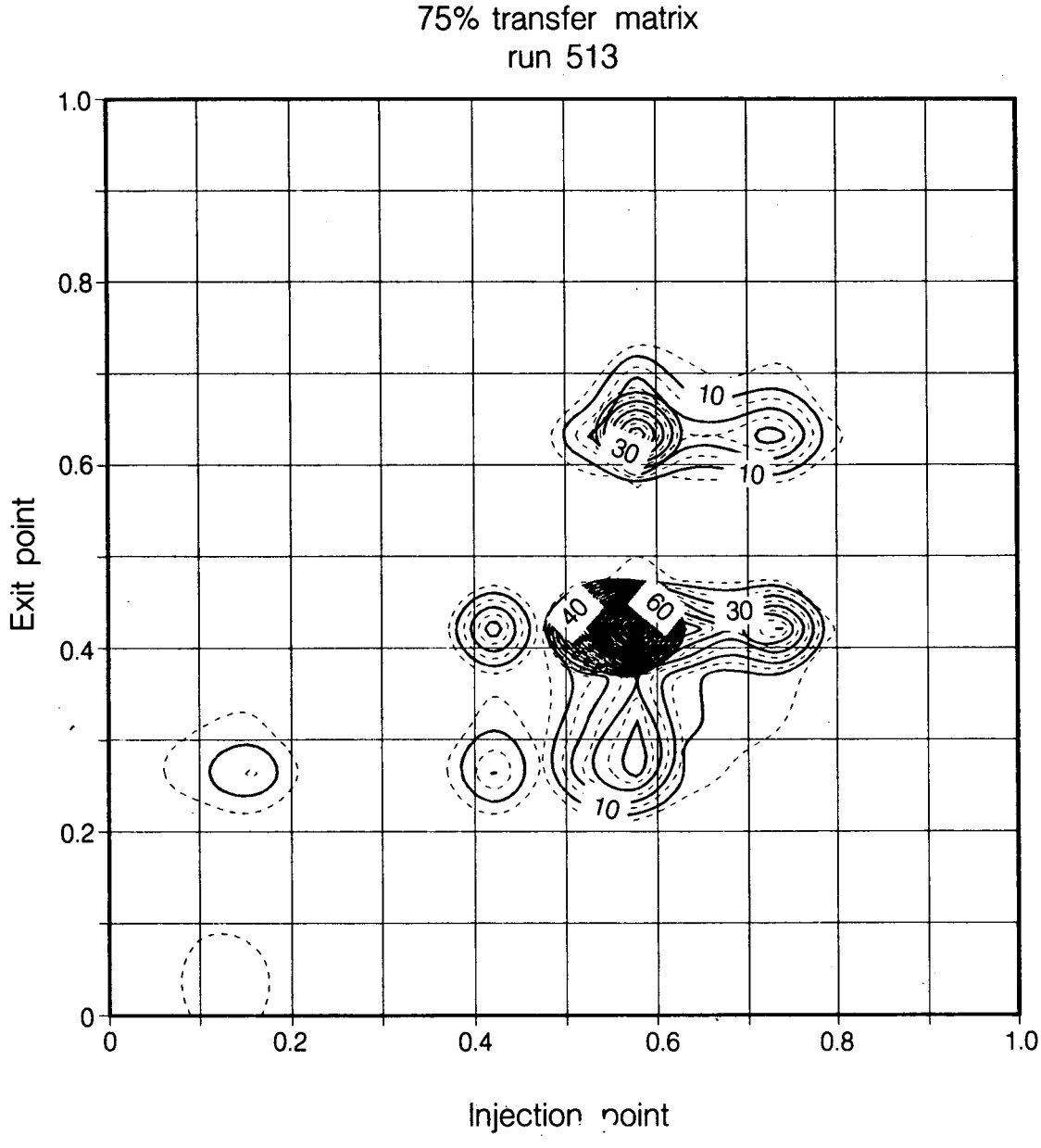

XBL 875-9676

Figure 8c. Contours of particle number density as a function of tracer entrance location and collection location, for a fracture with aperture variation as shown in Figure 1c at $t_{.75}$, when 75 % of the input particles have arrived at the exit boundary.

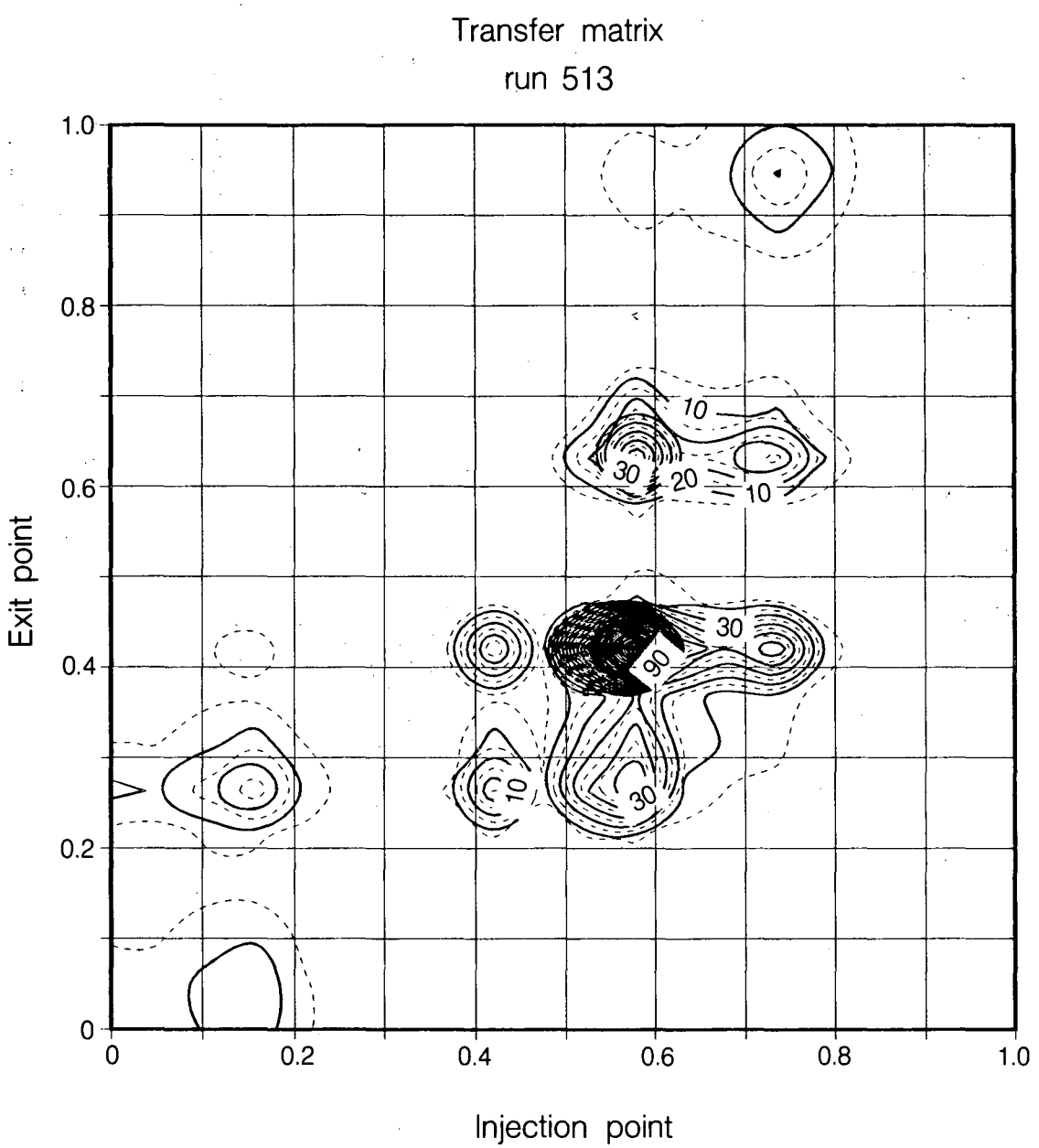

XBL 875-9677

Figure 8d. Contours of particle number density as a function of tracer entrance location and collection location, for a fracture with aperture variation as shown in Figure 1c at $t_{1.0}$, when 100 % of the input particles have arrived at the exit boundary.

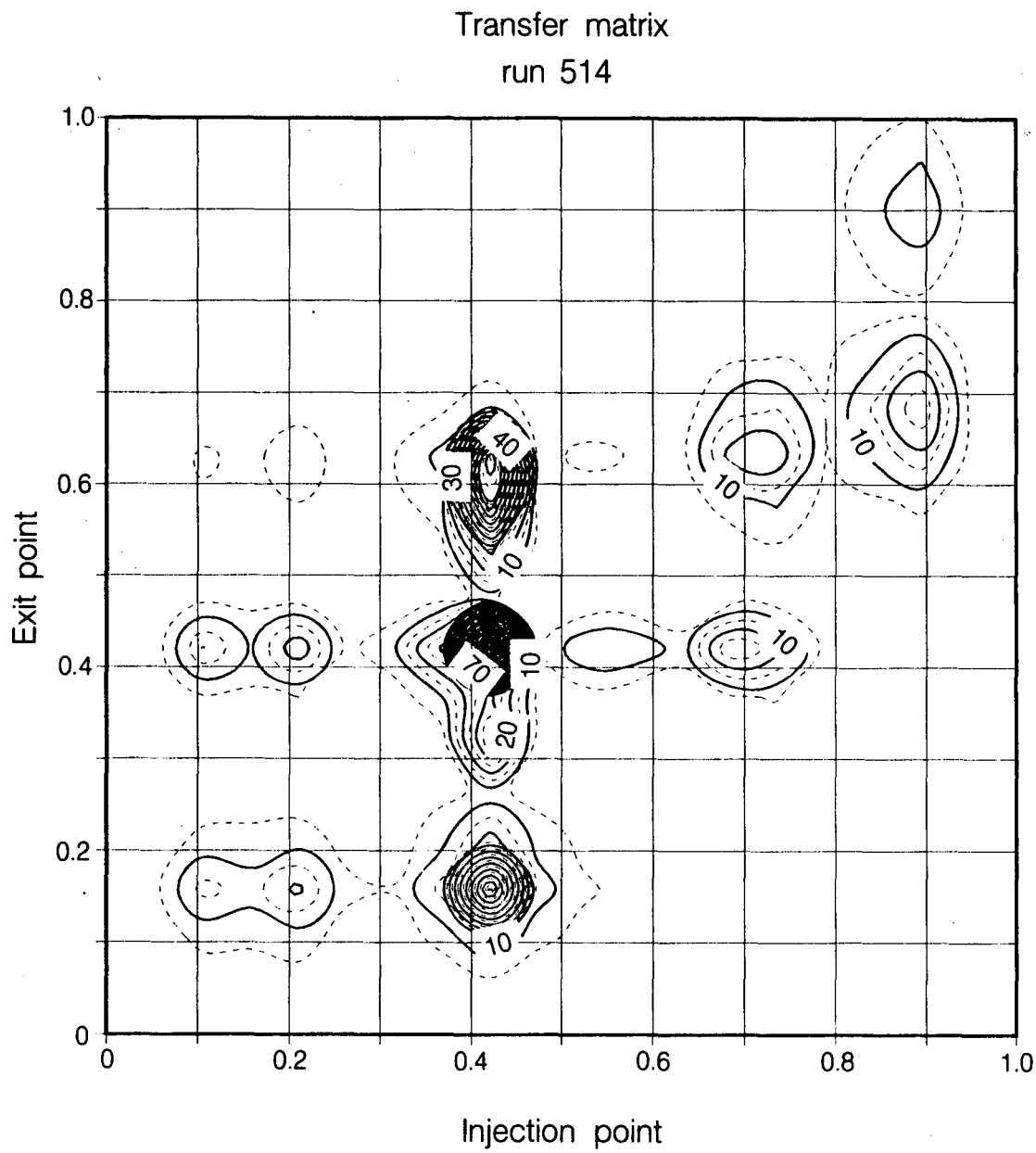

Figure 9. Contours of particle number density as a function of tracer entrance location and collection location, for a fracture with aperture variation as shown in Figure 1d.

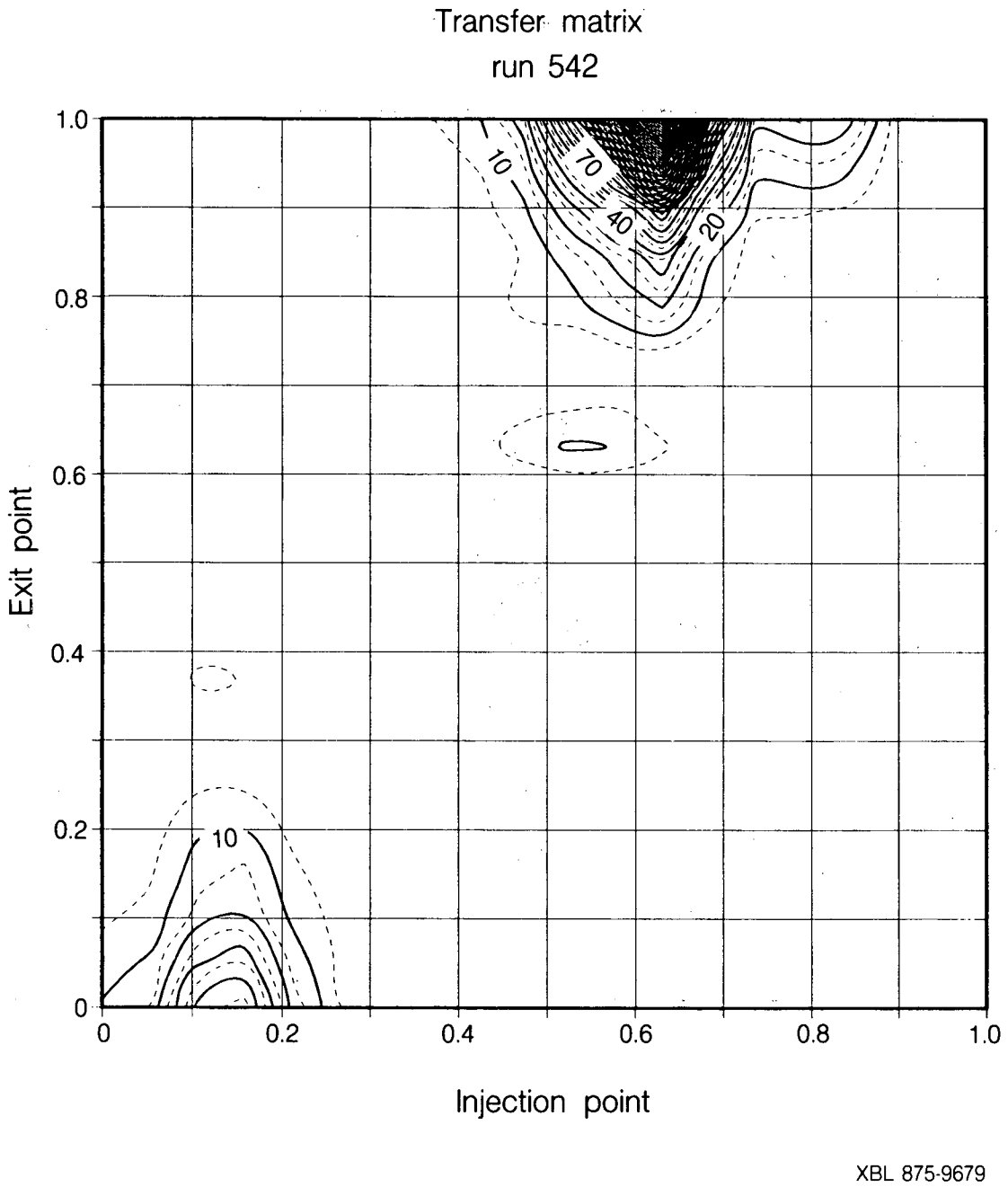

Figure 10. Contours of particle number density as a function of tracer entrance location and collection location, for a fracture with aperture variation as shown in Figure 2b.

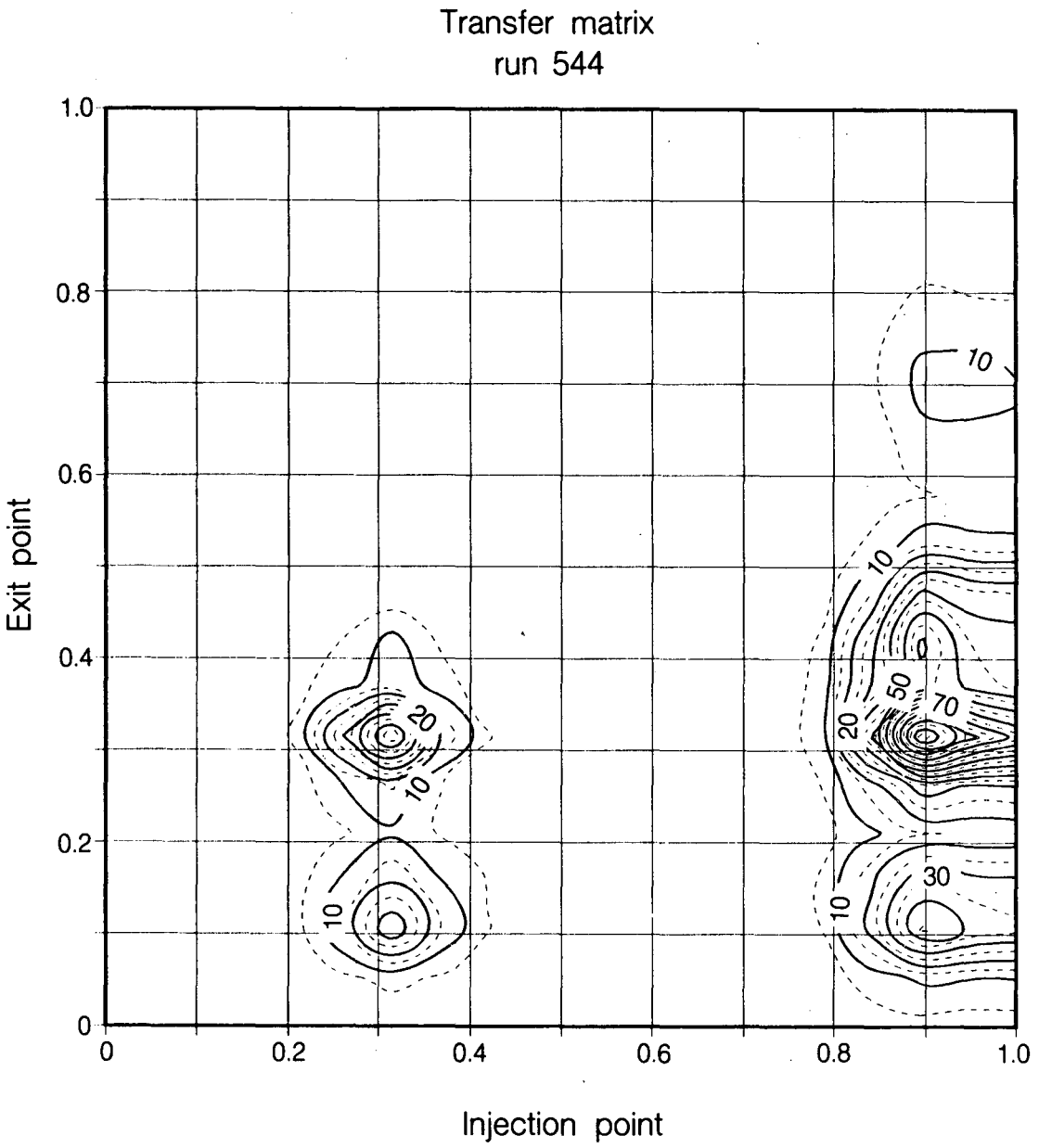

Figure 11. Contours of particle number density as a function of tracer entrance location and collection location, for a fracture with aperture variation as shown in Figure 2d.

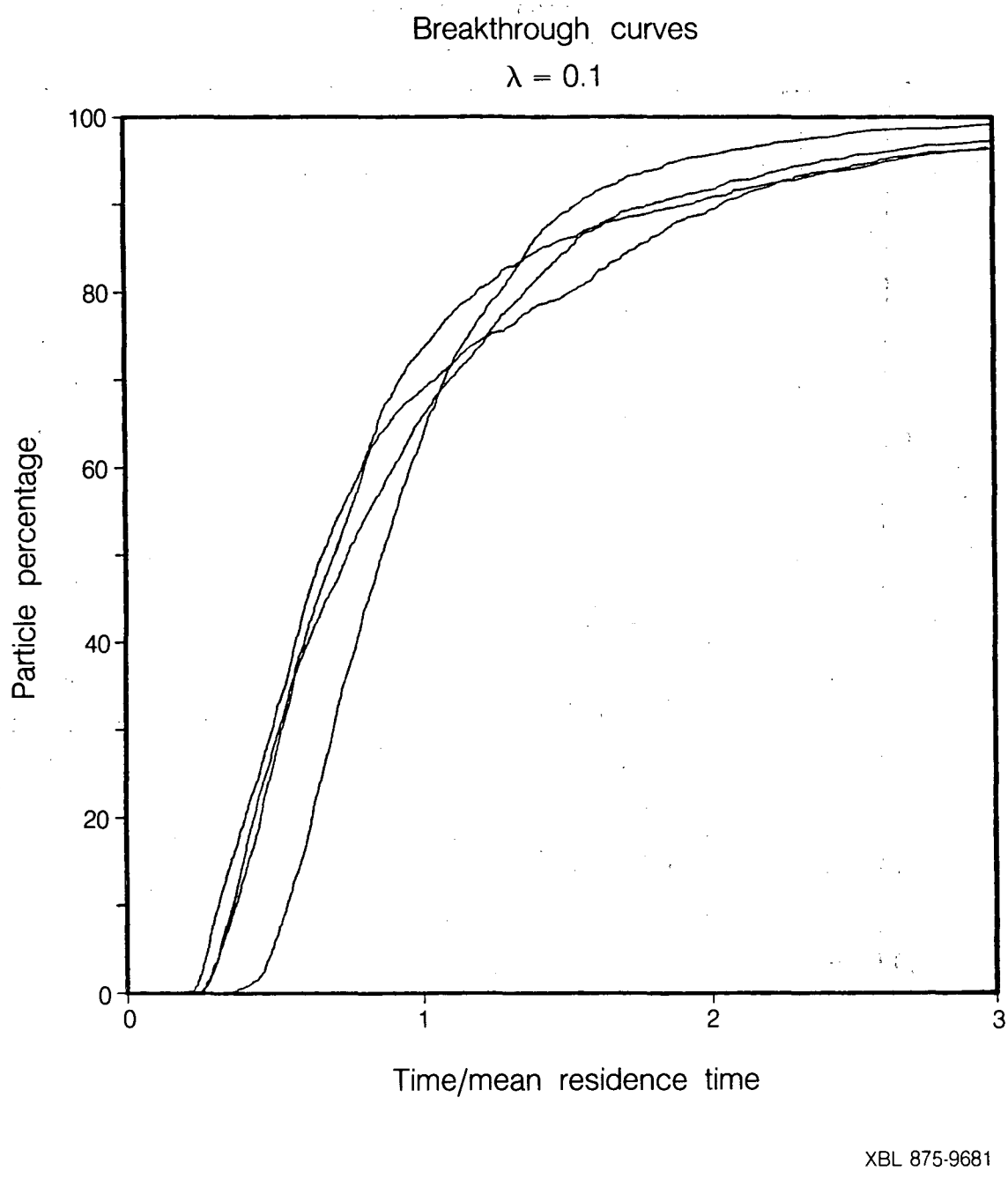

Figure 12. Tracer breakthrough curves from particle tracking in fractures with correlation length 0.1. Time is normalized to mean residence time, t_m.

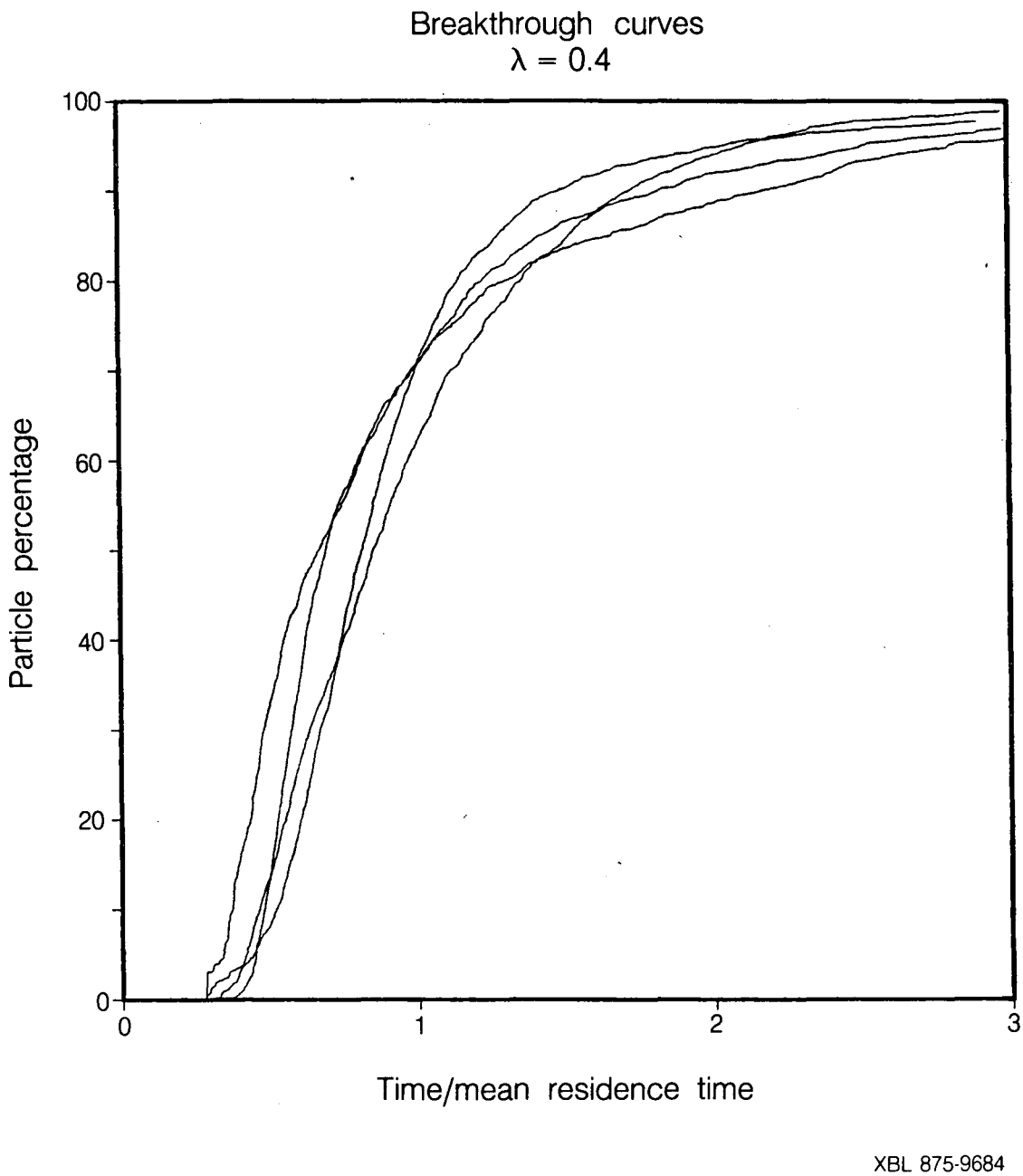

Figure 13. Tracer breakthrough curves from particle tracking in fractures with correlation length 0.4. Time is normalized to mean residence time, t_m.

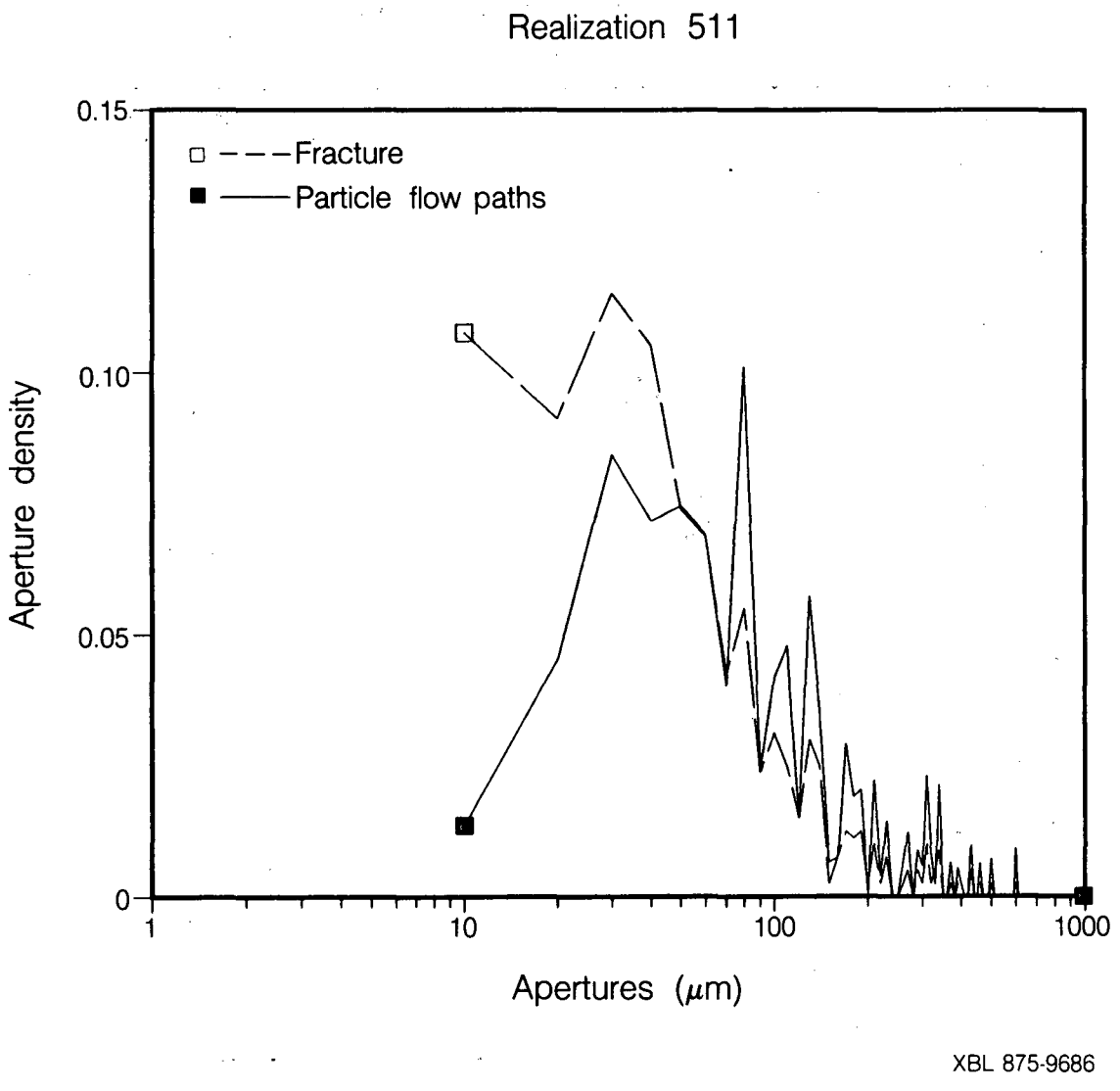

Figure 14. The aperture density distributions for apertures along particle paths, and over the entire fracture of Figure 1a.

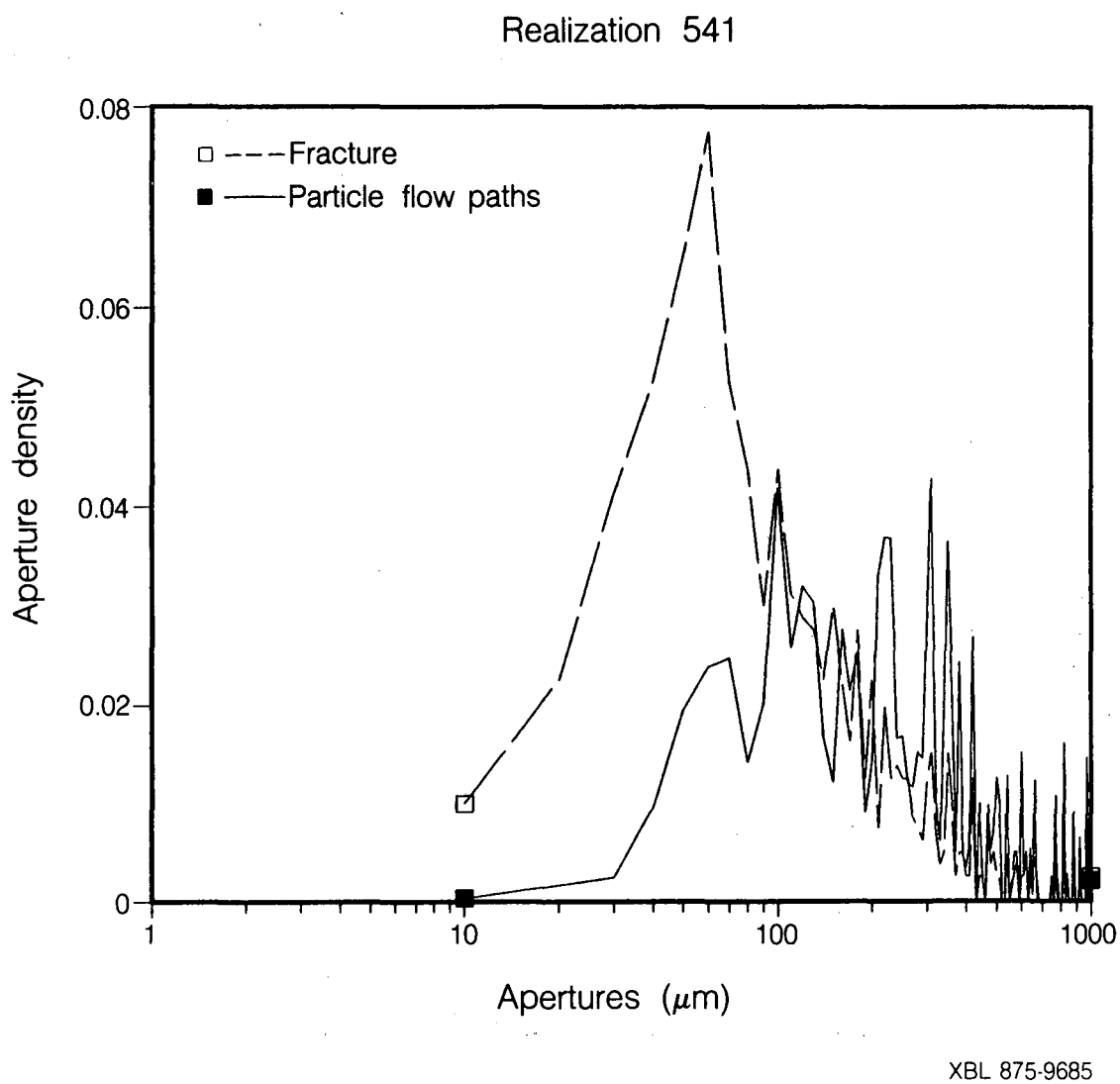

Figure 15. The aperture density distribution for apertures along particle paths, and over the entire fracture of Figure 2a.

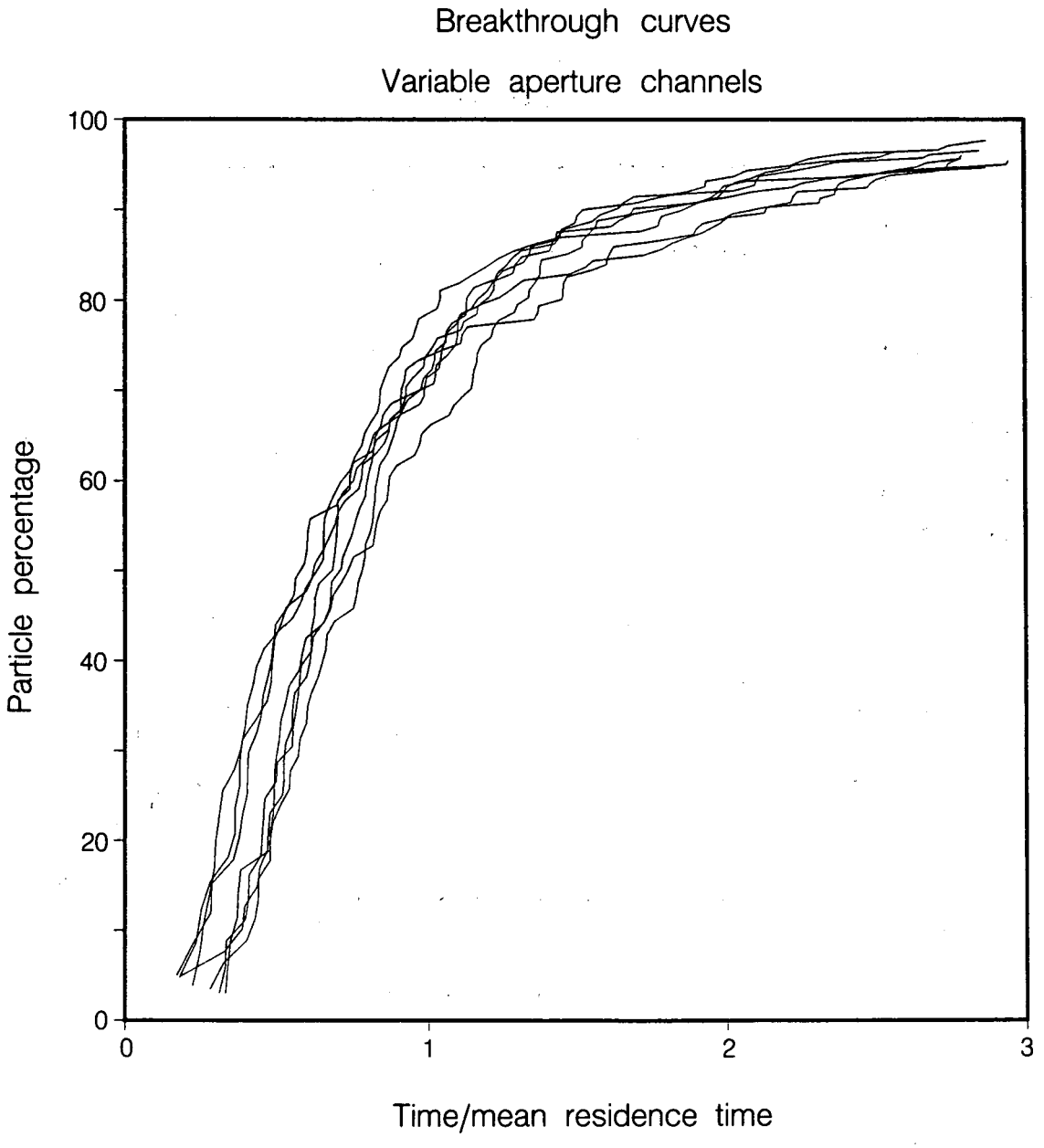

XBL 875-9682

Figure 16. Tracer breakthrough curves from one-dimensional variable-aperture channel calculations for the seven realizations of apertures as shown in Figure 1 and 2.

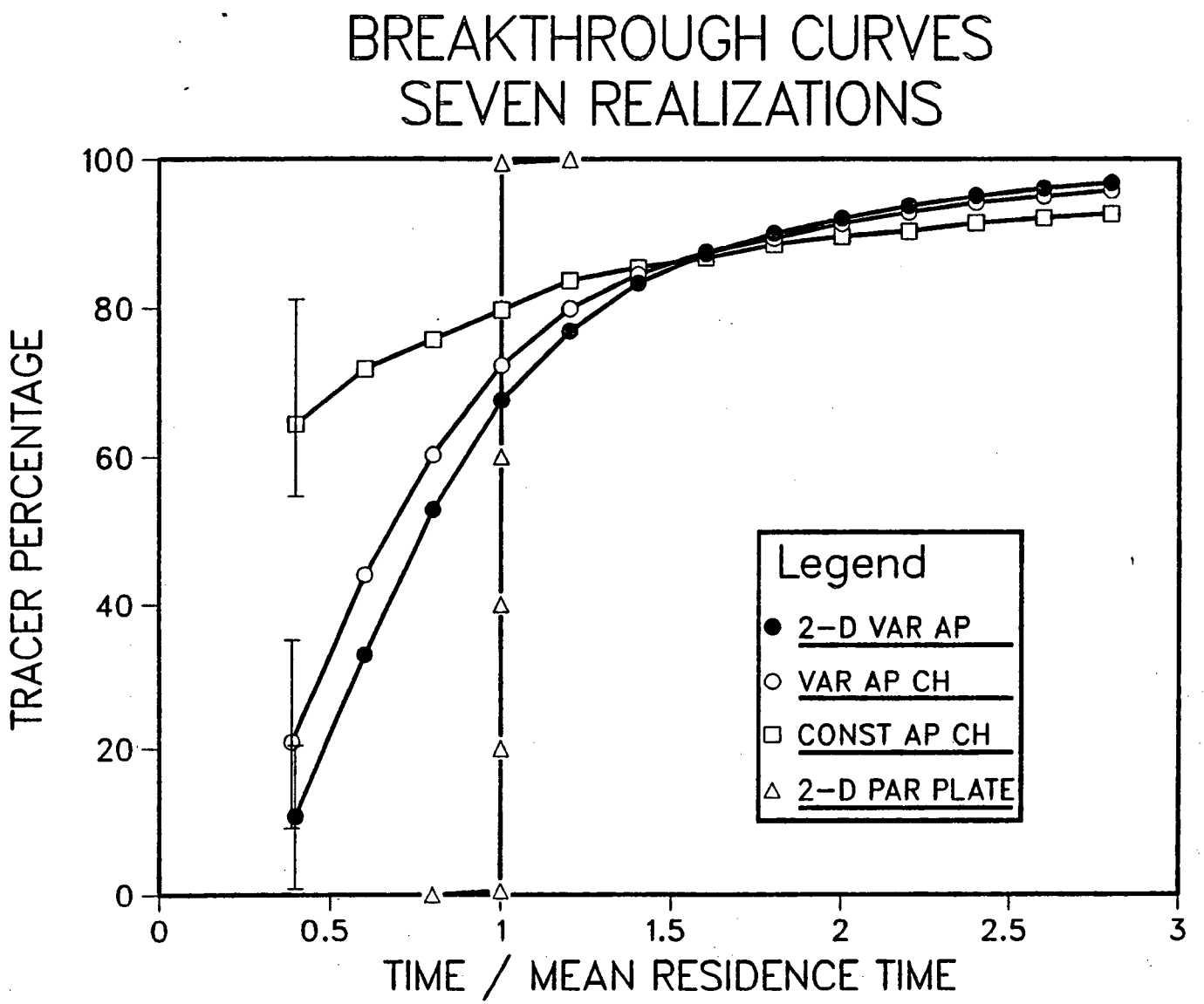

Figure 17. Tracer breakthrough curves from two-dimensional calculation (●), one-dimensional variable-aperture channel calculation (O), constant-aperture channel calculation (□), and parallel-plate fracture calculation (Δ). Vertical bars give limits of values from different realizations.

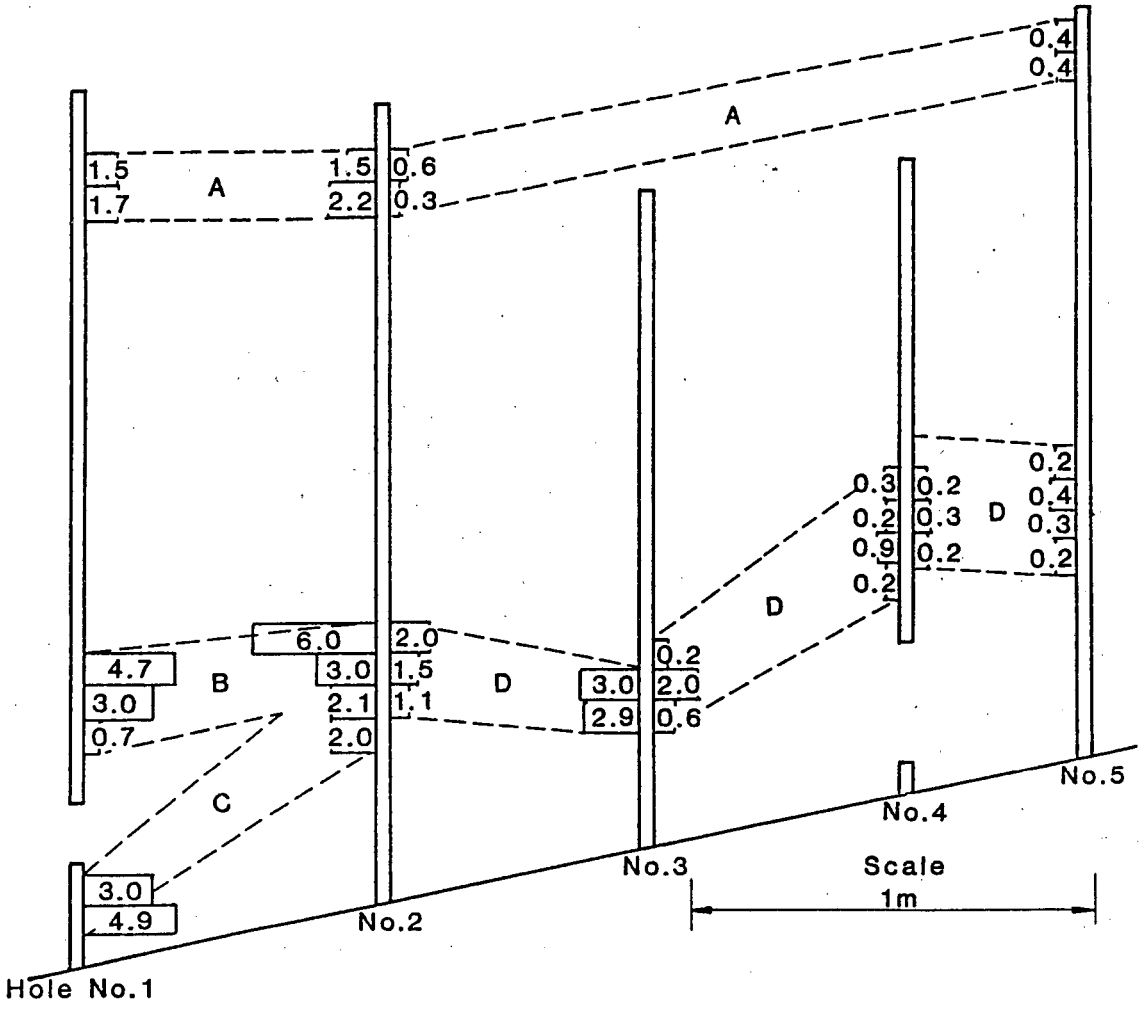

Numbers on histograms are flows in ml/sec from adjacent holes

Figure 18. Plan view of fracture with flows into five boreholes and suggested flow channels (Bourke,1987).

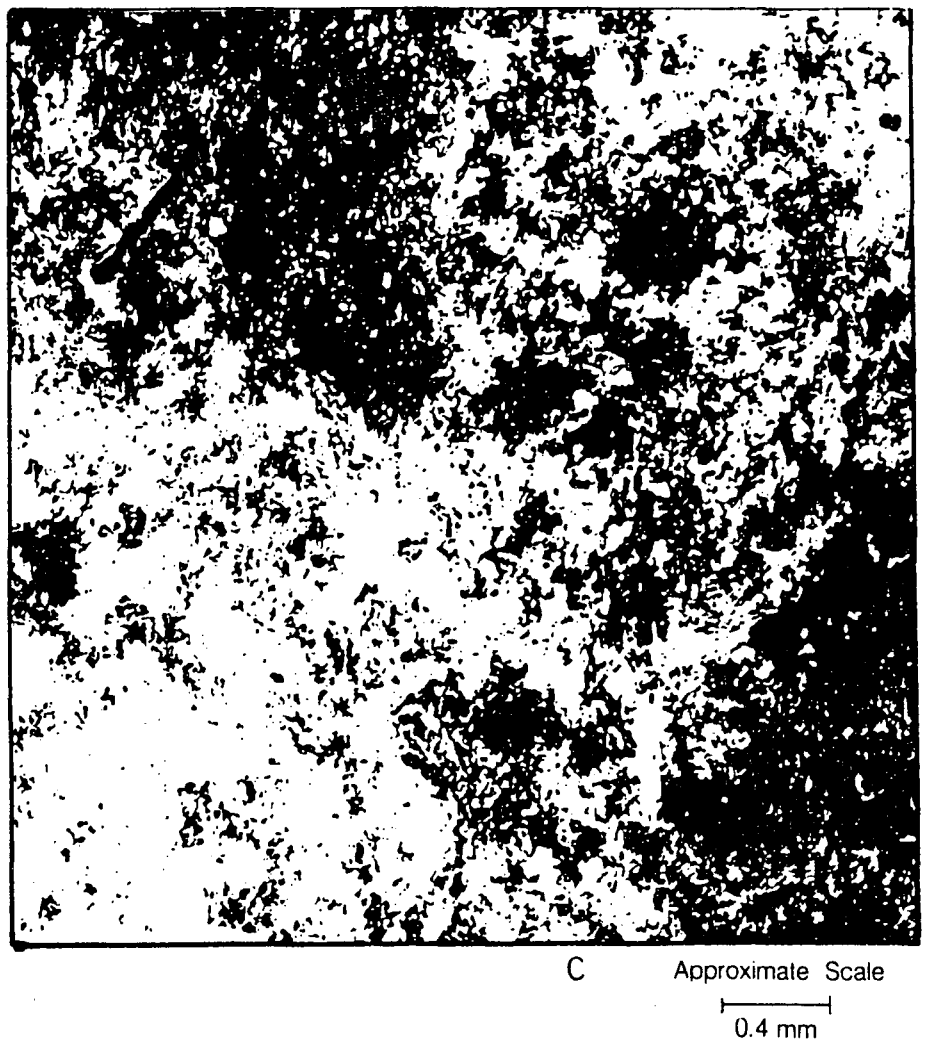

Figure 19. Compositive from SEM micrographs of fracture surfaces (Pyrak-Nolte et al., 1987).

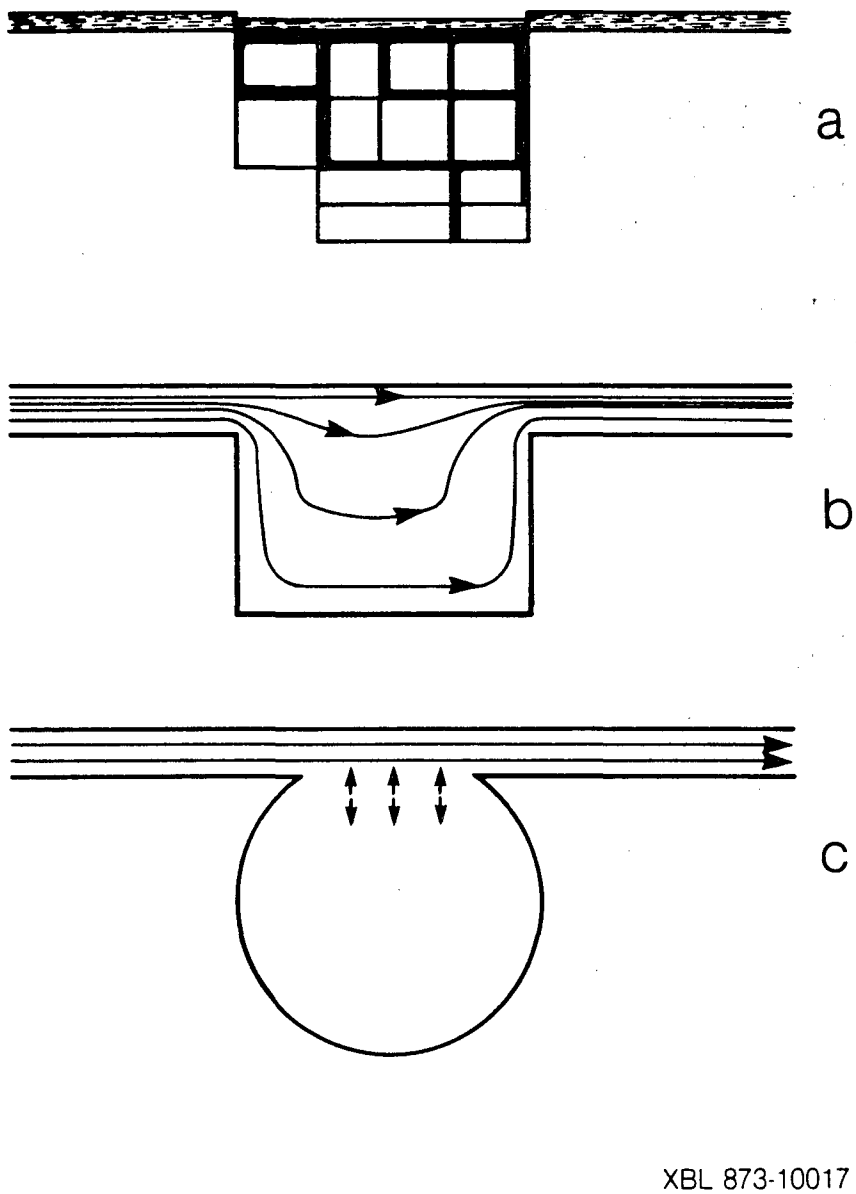

Figure 20. (a) Representation of flow "pool" in the electrical resistor analog.
(b) Pools of water with flow stream lines.
(c) Stagnant "pool" of water, having diffusive exchange with flow lines.

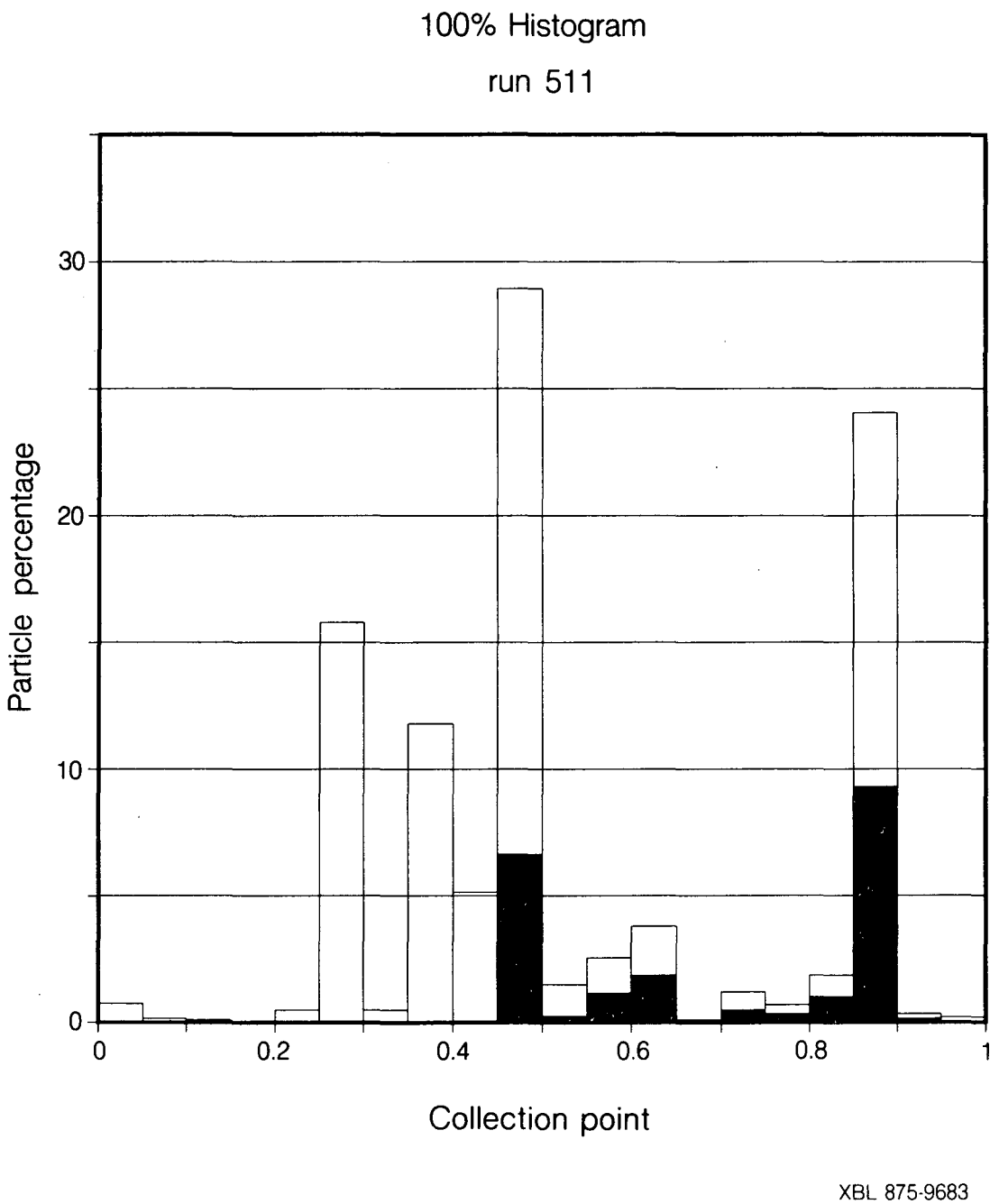

Figure 21. Histogram of flowrate (unfilled bars) and particle number (filled bars) as a function of exit location.

This report was done with support from the Department of Energy. Any conclusions or opinions expressed in this report represent solely those of the author(s) and not necessarily those of The Regents of the University of California, the Lawrence Berkeley Laboratory or the Department of Energy.

Reference to a company or product name does not imply approval or recommendation of the product by the University of California or the U.S. Department of Energy to the exclusion of others that may be suitable.

LAWRENCE BERKELEY LABORATORY
TECHNICAL INFORMATION DEPARTMENT
UNIVERSITY OF CALIFORNIA
BERKELEY, CALIFORNIA 94720